J. Fluid Mech. (2005), *vol.* 526, *pp.* 217–243. © 2005 Cambridge University Press
DOI: 10.1017/S0022112004002769 Printed in the United Kingdom

Nonlinear effects in reflecting and colliding internal wave beams

By ALI TABAEI[1], T. R. AKYLAS[2] AND KEVIN G. LAMB[3]

[1]Department of Civil & Environmental Engineering, Massachusetts Institute of Technology, Cambridge, MA 02139, USA

[2]Department of Mechanical Engineering, Massachusetts Institute of Technology, Cambridge, MA 02139, USA

[3]Department of Applied Mathematics, University of Waterloo, Ontario, Canada N2L 3G1

(Received 26 February 2004 and in revised form 5 October 2004)

Using small-amplitude expansions, we discuss nonlinear effects in the reflection from a sloping wall of a time-harmonic (frequency ω) plane-wave beam of finite cross-section in a uniformly stratified Boussinesq fluid with constant buoyancy frequency N_0. The linear solution features the incident and a reflected beam, also of frequency ω, that is found on the same (opposite) side to the vertical as the incident beam if the angle of incidence relative to the horizontal is less (greater) than the wall inclination. As each of these beams is an exact nonlinear solution, nonlinear interactions are confined solely in the vicinity of the wall where the two beams meet. At higher orders, this interaction region acts as a source of a mean and higher-harmonic disturbances with frequencies $n\omega$ $(n = 2, 3, \ldots)$; for $n\omega < N_0$ the latter radiate in the far field, forming additional reflected beams along $\sin^{-1}(n\omega/N_0)$ to the horizontal. Depending on the flow geometry, higher-harmonic beams can be found on the opposite side of the vertical from the primary reflected beam. Using the same approach, we also discuss collisions of two beams propagating in different directions. Nonlinear interactions in the vicinity of the collision region induce secondary beams with frequencies equal to the sum and difference of those of the colliding beams. The predictions of the steady-state theory are illustrated by specific examples and compared against unsteady numerical simulations.

1. Introduction

In a recent paper (Tabaei & Akylas 2003), it was pointed out that the effects of nonlinearity are relatively insignificant in the propagation of finite-amplitude internal gravity-wave beams in a uniformly stratified Boussinesq fluid with constant Brunt–Väisälä frequency N_0. Under these flow conditions, a uniform plane-wave beam of frequency ω obeying the linear dispersion relation

$$\omega^2 = N_0^2 \sin^2\theta, \tag{1.1}$$

θ being the beam inclination relative to the horizontal, satisfies the nonlinear governing equations of motion irrespective of its cross-sectional profile. Moreover, for a beam that is slowly modulated along the beam direction, the leading-order nonlinear effects owing to the modulations happen to cancel out. The propagation of an isolated finite-amplitude internal wave beam in a Boussinesq fluid is thus controlled predominantly by dispersive, viscous and possibly refraction effects brought about by variations of the Brunt–Väisälä frequency and the presence of a background mean flow.

https://doi.org/10.1017/S0022112004002769 Published online by Cambridge University Press

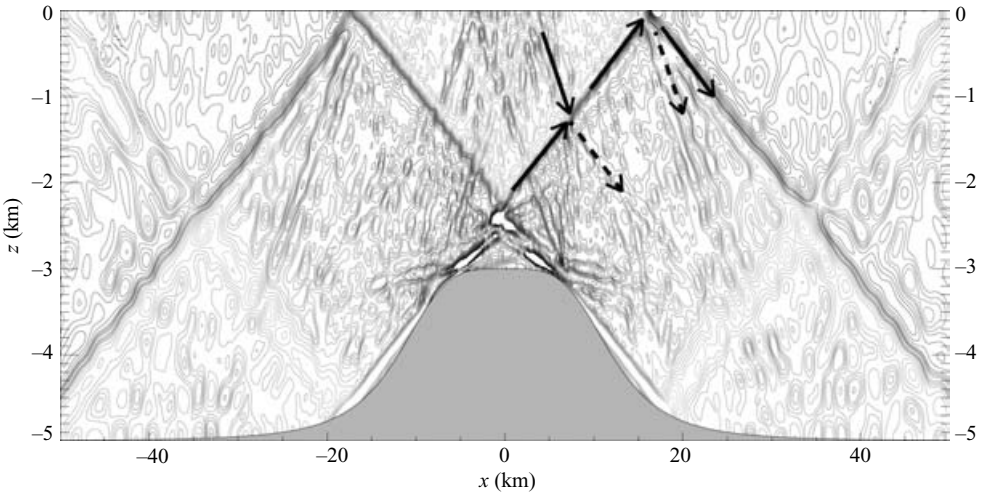

FIGURE 1. Contour plot of the horizontal velocity field generated by on oscillating tidal flow over a two-dimensional ridge after 12 tidal periods (Lamb 2004). The background stratification used had constant buoyancy frequency $N = 10^{-3}\,\mathrm{rad\,s^{-1}}$ and the Coriolis frequency was $f = 0.5 \times 10^{-4}\,\mathrm{rad\,s^{-1}}$. A reflection of a primary-harmonic beam (tidal frequency) from the upper boundary and a collision of primary- and second-harmonic beams are highlighted by arrows. Dashed arrows indicate secondary beams generated by nonlinear interactions.

Here we consider interactions of two plane-wave beams propagating along different directions. In this instance, unlike the case of an isolated wave beam, nonlinear effects turn out to be particularly important.

The original motivation for the present work came from numerical simulations of stratified oscillatory flow over topography in a channel of finite depth (Lamb 2004). Bell (1975) studied the analogous infinite-depth problem, when no upper boundary is present, and noted that the linear response comprises a finite number of time-harmonic wave beams radiating outwards from the topography with frequencies equal to that of the background flow and its higher harmonics below the Brunt–Väisälä frequency. In finite-depth flow, as seen in Lamb (2004), these beams reflect from the upper boundary and subsequently interact with the flow field in a manner which brings out the significance of nonlinear effects.

As an illustration of the simulations of Lamb (2004), figure 1 shows a snapshot of the generated disturbance after 12 oscillation periods of the background flow. As expected, wave beams with the frequency of the background flow and its second harmonic are clearly visible over the topography and by this time have reflected from the upper wall. Note, however, that nonlinear effects play an important part in the course of these reflections: apart from a reflected wave beam with the same frequency as the incident wave beam in accordance with the linear theory, the numerical simulations reveal a secondary reflected beam having twice the incident frequency and propagating closer to the vertical, consistent with the dispersion relation (1.1).

Moreover, according to figure 1, collisions of wave beams exhibit interesting properties owing to nonlinear effects. Unlike linear wave beams which can be superposed and, hence, emerge intact from collisions, the numerical simulations suggest that collisions of two nonlinear beams give rise to additional beams of frequencies equal to the sum and difference of the frequencies of the colliding beams. While the collisions seen in figure 1 involve beams with the background-flow frequency and its

https://doi.org/10.1017/S0022112004002769 Published online by Cambridge University Press

second harmonic, it is anticipated that, in general, collisions among nonlinear beams of different frequencies feature analogous properties.

Using small-amplitude expansions, here we present an analytical treatment of nonlinear effects in reflecting and colliding wave beams. Rather than reflections from a horizontal wall, we discuss the more general problem of a wave beam reflecting from a sloping wall. The linear solution is analogous to that given in Phillips (1966, § 5.5) for the reflection of a plane wave and features a single reflected beam having the same frequency as the incident beam; the two beams are found either on the same side or on opposite sides of the vertical, respectively, when the angle of incidence, measured from the horizontal, is smaller or greater than the wall inclination.

Thorpe (1987) obtained nonlinear corrections to the linear solution for the reflection of a plane wave from a sloping wall and identified certain resonances near which nonlinear effects are more pronounced. In the case of a reflecting wave beam of finite cross-section, however, nonlinear effects manifest themselves in a different way, as nonlinear interactions here are confined solely to the vicinity of the wall where the incident and reflected beams of the linear solution meet.

At higher orders, this region acts as a source of a mean flow and oscillatory disturbances with frequencies equal to the higher harmonics of the incident frequency. While the induced mean flow turns out to remain always locally confined, the higher-harmonic disturbances radiate in the far field, forming additional reflected beams, for all harmonics below the Brunt–Väisälä frequency. To determine the direction of propagation and the profile of each of these reflected beams, we invoke a radiation condition which ensures that the response is causal. In certain flow geometries, in particular, we find that higher-order reflected beams propagate on the opposite side of the vertical from the primary reflected beam. We remark that, in their numerical simulations of wave-beam reflection from a sloping boundary, Javam, Imberger & Armfield (1999) noted the presence of higher harmonics, owing to nonlinear interactions, in the overlap region of the incident and reflected beams; however, all the higher-harmonic frequencies happened to be greater than the buoyancy frequency, precluding radiation of additional beams.

Following a similar perturbation approach, we also demonstrate that, when two wave beams of different frequencies collide, nonlinear interactions in the region where the two beams overlap give rise to higher-order disturbances with frequencies equal to sums and differences of the two primary harmonics. These disturbances radiate outwards from the interaction region, forming secondary beams, if the corresponding frequency is less than the Brunt–Väisälä frequency. Laboratory experiments (Chashechkin & Neklyudov 1990; Teoh, Ivey & Imberger 1997) and numerical simulations (Javam, Imberger & Armfield 2000) confirm that nonlinear interactions excite combinations of the two primary harmonics within the collision region; little attention has been paid in prior work, however, to the resulting radiation of secondary beams when some of the excited frequencies are below the buoyancy frequency.

In problems of weakly nonlinear wave interactions, nonlinear effects are usually most pronounced under conditions for which the interaction occurs over long distance and time, this being the case when the waves travel in almost the same direction and with nearly equal speed. In the case of interacting wave beams, however, it appears that the opposite is true: as pointed out in Tabaei & Akylas (2003), nonlinear effects in the interaction of wave beams propagating along nearly coincident directions turn out to be relatively insignificant. On the other hand, as demonstrated below, nonlinear interactions of beams propagating along different directions can have quite dramatic effects.

https://doi.org/10.1017/S0022112004002769 Published online by Cambridge University Press

2. Preliminaries

We shall consider interactions among plane internal gravity-wave beams in the simplest case of inviscid, incompressible, uniformly stratified Boussinesq flow. Under these flow conditions, employing the same scalings as in Tabaei & Akylas (2003), the governing equations, in dimensionless form, are

$$\nabla \cdot \boldsymbol{u} = 0, \tag{2.1}$$

$$\rho_t + \boldsymbol{u} \cdot \nabla \rho - v = 0, \tag{2.2}$$

$$\boldsymbol{u}_t + \boldsymbol{u} \cdot \nabla \boldsymbol{u} = -\nabla p - \rho \boldsymbol{j}, \tag{2.3}$$

where $\boldsymbol{u} = (u, v)$ is the velocity field, p and ρ are the reduced pressure and density, respectively, and $\boldsymbol{j}$ is a unit vector pointing upwards along the vertical (y-) direction. The Brunt–Väisälä frequency is constant under the assumptions made here and has been normalized to unity.

Introducing a streamfunction ψ, such that $u = \psi_y$ and $v = -\psi_x$, the incompressibility condition (2.1) is automatically satisfied; the mass-conservation equation (2.2) and the momentum equation (2.3), after eliminating the pressure p, then take the form

$$\rho_t + \psi_x + J(\rho, \psi) = 0, \tag{2.4}$$

$$\nabla^2 \psi_t - \rho_x + J(\nabla^2 \psi, \psi) = 0, \tag{2.5}$$

where $J(a, b) = a_x b_y - a_y b_x$ stands for the Jacobian.

An interesting feature of internal gravity waves, which stems from the anisotropic nature of this type of wave motion, is that the frequency ω of a sinusoidal plane wave depends only on the orientation of the wavenumber vector $\boldsymbol{k} = k(\sin\theta, \cos\theta)$, but not its magnitude, as indicated by the dispersion relation (1.1) which takes the dimensionless form

$$\omega^2 = \sin^2\theta. \tag{2.6}$$

As explained in Tabaei & Akylas (2003), this property makes it possible to construct, via superposition of sinusoidal plane waves with wavenumbers inclined at the same angle θ to the vertical, general plane-wave disturbances of frequency ω, in the form of beams, that are uniform along $\xi = x\cos\theta - y\sin\theta$ and have a general profile along $\eta = x\sin\theta + y\cos\theta$:

$$\psi = Q(\eta)\, \mathrm{e}^{-\mathrm{i}\omega t} + \text{c.c.}, \tag{2.7}$$

$$(\rho, p) = (-\mathrm{i}\, Q_\eta,\ \mathrm{i}\cos\theta\, Q)\, \mathrm{e}^{-\mathrm{i}\omega t} + \text{c.c.}, \tag{2.8}$$

where $Q(\eta)$ is a complex amplitude and c.c. denotes the complex conjugate. Moreover, as the velocity $\boldsymbol{u}$ is in the ξ-direction along which no variations are present, this class of disturbances satisfies the full nonlinear equations of motion as well.

As is well known, in the solution of steady-wave problems, it is necessary to impose suitable radiation conditions, ensuring that the solution is causal. In the present setting, in particular, all beams resulting from the reflection of a wave beam incident on a wall and from the collision of two beams must be such that they transport energy outwards from the region of interaction.

In general, the direction of energy propagation is along the group velocity $\boldsymbol{c}_g = \nabla_{\boldsymbol{k}}\, \omega$ which, according to the dispersion relation (2.6), here turns out to be orthogonal to the phase velocity $\boldsymbol{c} = (\omega/k^2)\, \boldsymbol{k}$; furthermore, it is easy to check that $\boldsymbol{c}_g$ and $\boldsymbol{c}$ have opposite vertical components. Four possible configurations of $\boldsymbol{c}_g$ and $\boldsymbol{c}$ thus arise,

https://doi.org/10.1017/S0022112004002769 Published online by Cambridge University Press

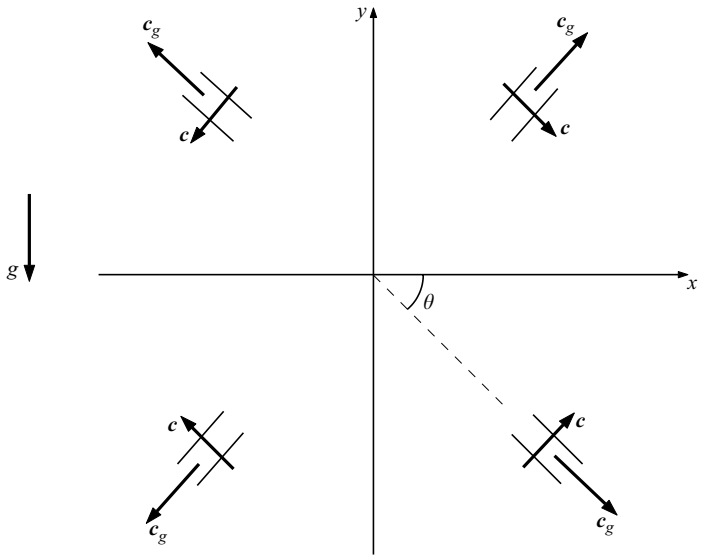

FIGURE 2. Four possible configurations of the group velocity $\boldsymbol{c}_g$ and phase velocity $\boldsymbol{c}$ of plane waves, with wavenumber vector inclined at an angle θ to the vertical, obeying the dispersion relation (2.6).

as shown in figure 2 for plane-wave disturbances radiating outwards from a region centred at the origin (see, for example, Lighthill 1978).

In view of the need to satisfy a radiation condition, it is also important to note that, while (2.7) and (2.8) describe plane-wave beams for any choice of the amplitude $Q(\eta)$, uni-directional beams, in which energy propagates in one direction, involve plane waves with wavenumbers of the same sign only. For example, according to figure 2, for $\omega > 0$ and $\boldsymbol{k} = k(\sin\theta,\ \cos\theta)$ with $0 < \theta < \pi/2$, taking $Q(\eta)$ to be a superposition of plane waves with $k > 0$,

$$Q(\eta) = \int_0^\infty A(k)\, \mathrm{e}^{\mathrm{i}k\eta}\, \mathrm{d}k, \tag{2.9}$$

where $A(k)$ denotes the Fourier transform of $\psi(\eta,\ t = 0)$, yields a wave beam in which energy propagates along the positive ξ-direction. On the other hand, if $Q(\eta)$ involves negative wavenumbers ($k < 0$),

$$Q(\eta) = \int_{-\infty}^0 A(k)\, \mathrm{e}^{\mathrm{i}k\eta}\, \mathrm{d}k, \tag{2.10}$$

energy propagates in the negative ξ-direction. This makes it clear that the wave beams considered by Kistovich & Chashechkin (1991) in their study of nonlinear wave-beam interactions, are not uni-directional.

An expression for the energy flux associated with a time-harmonic wave beam can be obtained as follows. Multiplying the horizontal component of the momentum equation (2.3) with u, the vertical component with v and the mass equation (2.2) with ρ, and then adding these equations, making use of (2.1), yields the conservation law

$$\tfrac{1}{2}(u^2 + v^2 + \rho^2)_t + \nabla\cdot\{\tfrac{1}{2}(u^2 + v^2 + \rho^2)\boldsymbol{u}\} + \nabla\cdot(p\boldsymbol{u}) = 0 \tag{2.11}$$

https://doi.org/10.1017/S0022112004002769 Published online by Cambridge University Press

for the sum of kinetic and potential energy. Focusing now on a time-harmonic wave beam of the form (2.7) and (2.8) and averaging over a time period, the average energy flux associated with such a disturbance is given by

$$\frac{1}{(2\pi/\omega)}\int_0^{2\pi/\omega} p\boldsymbol{u}\,\mathrm{d}t;$$

hence, integrating across the beam, the average energy flow rate in a beam of finite cross-section is

$$\mathscr{F} = \mathrm{i}\cos\theta\int_{-\infty}^{\infty}(Q^*Q_\eta - Q\,Q_\eta^*)\,\mathrm{d}\eta = 2\mathrm{i}\cos\theta\int_{-\infty}^{\infty}Q^*Q_\eta\,\mathrm{d}\eta, \tag{2.12}$$

where $*$ denotes complex conjugate. Note that the integrals above are imaginary so the expression for $\mathscr{F}$ is real.

According to (2.12), the energy flow rate in a beam inclined at an angle θ to the horizontal is proportional to $\cos\theta$, as is the group velocity which controls energy propagation. Furthermore, note that $\mathscr{F}=0$ when the beam amplitude profile $Q(\eta)$ happens to be real; this is to be expected, as $Q(\eta)$ then is a superposition of (2.9) and (2.10) so equal amounts of energy propagate in the positive and the negative ξ-directions, resulting in a standing wave confined in the η-direction.

We shall employ expression (2.12) for the average energy flow rate in a beam when we discuss in § 4 how the energy of a beam incident on a sloping wall is partitioned among the reflected beams. In addition, conservation of energy will be used to check our computations of reflections and collisions of weakly nonlinear beams in § 6.

3. Reflection from a uniform slope

Consider a plane-wave beam incident at an angle θ to the horizontal on a slope of angle α. According to the dispersion relation (2.6), the incident frequency is $\omega = \sin\theta$. We wish to determine the steady-state reflected wave field taking into account weakly nonlinear effects. To this end, we shall use expansions in terms of an amplitude parameter, $\epsilon \ll 1$. In the following, it will be assumed that $0<\theta<\pi/2$; details for other angles of incidence can be worked out in a similar fashion.

It is convenient to rotate axes so that x is along and y is normal to the slope (see figure 3). In the new coordinate system, the governing equations (2.4) and (2.5) are slightly more complicated:

$$\rho_t + \cos\alpha\,\psi_x - \sin\alpha\,\psi_y + J(\rho,\psi) = 0, \tag{3.1}$$

$$\nabla^2\psi_t - \cos\alpha\,\rho_x + \sin\alpha\,\rho_y + J(\nabla^2\psi,\psi) = 0; \tag{3.2}$$

however, the wall boundary condition, that the velocity component normal to the slope must vanish, takes the simple form

$$\psi_x = 0 \quad (y=0). \tag{3.3}$$

The linear solution is analogous to that for a plane wave reflecting from a slope (Phillips 1966, § 5.5):

$$\psi = \epsilon\,Q(x,y)\,\mathrm{e}^{-\mathrm{i}\omega t} + \text{c.c.}, \tag{3.4a}$$

$$\rho = -\frac{\mathrm{i}}{\omega}\epsilon(\cos\alpha\,Q_x - \sin\alpha\,Q_y)\,\mathrm{e}^{-\mathrm{i}\omega t} + \text{c.c.}, \tag{3.4b}$$

https://doi.org/10.1017/S0022112004002769 Published online by Cambridge University Press

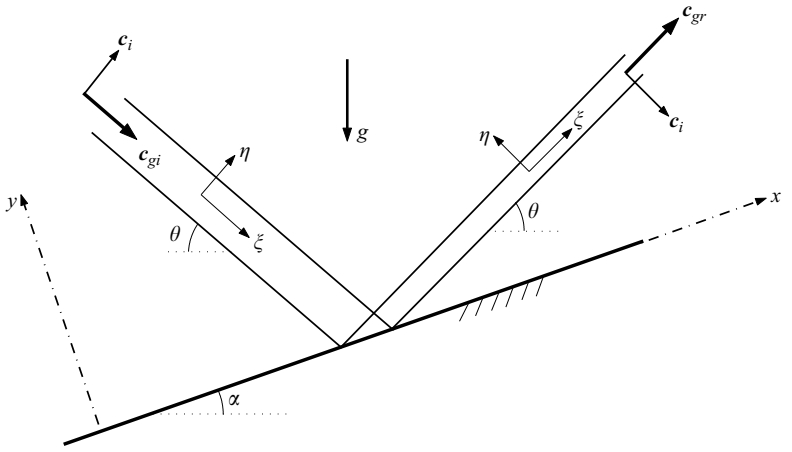

FIGURE 3. Incident and reflected wave beams from a slope of inclination α, according to linear theory; subscripts i and r denote incident and reflected beam, respectively. These beams comprise plane waves with group ($\boldsymbol{c}_g$) and phase ($\boldsymbol{c}$) velocities obeying the radiation conditions shown in figure 2. The reflected beam is found upslope when the angle of incidence $\theta > \alpha$ (as is the case shown here) and downslope when $\theta < \alpha$.

where

$$Q = Q^{\mathrm{inc}} + Q^{\mathrm{refl}}, \tag{3.5}$$

$$Q^{\mathrm{inc}}(x, y) = \int_0^\infty \mathrm{d}l\, A(l)\, \exp\{\mathrm{i}\, l(x + y\, \cot(\theta + \alpha))\}, \tag{3.6a}$$

being the amplitude profile of the incoming beam and

$$Q^{\mathrm{refl}}(x, y) = -\int_0^\infty \mathrm{d}l\, A(l)\, \exp\{\mathrm{i}\, l(x - y\, \cot(\theta - \alpha))\} \tag{3.6b}$$

the amplitude profile of the reflected beam. Clearly, the sum $Q^{\mathrm{inc}} + Q^{\mathrm{refl}}$ satisfies the boundary condition (3.3).

The incoming wave beam in (3.6*a*) involves plane waves with positive horizontal and vertical wavenumber components so the group velocity is directed towards the slope, as demanded by the radiation condition (see figure 2). The direction of the reflected beam in (3.6*b*), on the other hand, depends on whether $\theta > \alpha$ or $\theta < \alpha$; in the former case, the reflected beam is found on the upslope side of the incident beam while in the latter case, it is found on the downslope side. In either case, however, the wavenumber direction is such that the reflected energy flux propagates outwards from the slope, consistent with the radiation condition.

In the special case $\theta = \alpha$, the reflected beam (3.6*b*) is singular. A similar singularity arises in the reflection of a periodic wave, and Dauxois & Young (1999) discuss how the singular behaviour near this critical angle can be healed by taking into account nonlinear, transient and viscous effects. In the following it is assumed that θ is not close to α.

To study the reflection of a weakly nonlinear beam, ψ and ρ are expanded as follows:

$$\begin{aligned}\psi = {} & \epsilon\{Q(x, y)\, \mathrm{e}^{-\mathrm{i}\omega t} + \mathrm{c.c.}\} + \epsilon^2\{Q_0(x, y) + (Q_2(x, y)\, \mathrm{e}^{-2\mathrm{i}\omega t} + \mathrm{c.c.})\} \\ & + \epsilon^3\{(Q_3(x, y)\, \mathrm{e}^{-3\mathrm{i}\omega t} + \mathrm{c.c.}) + (Q_1(x, y)\, \mathrm{e}^{-\mathrm{i}\omega t} + \mathrm{c.c.})\} + \cdots,\end{aligned} \tag{3.7}$$

https://doi.org/10.1017/S0022112004002769 Published online by Cambridge University Press

$$\rho = \epsilon\{R(x,y)\,\mathrm{e}^{-\mathrm{i}\omega t} + \text{c.c.}\} + \epsilon^2\{R_0(x,y) + (R_2(x,y)\,\mathrm{e}^{-2\mathrm{i}\omega t} + \text{c.c.})\} + \epsilon^3\{(R_3(x,y)\,\mathrm{e}^{-3\mathrm{i}\omega t} + \text{c.c.}) + (R_1(x,y)\,\mathrm{e}^{-\mathrm{i}\omega t} + \text{c.c.})\} + \cdots, \tag{3.8}$$

the leading-order terms corresponding to the linear solution (3.4).

As usual in problems of wave interactions, the above expansions anticipate that nonlinear corrections to the reflected wave field introduce higher harmonics and a mean term. As already remarked, however, here the incident wave beam and the leading-order reflected beam happen to be nonlinear solutions so nonlinear interactions are confined solely in the vicinity of the slope where these beams overlap. This interaction region acts as a source of mean (Q_0 and R_0) and higher-harmonic ($Q_n\mathrm{e}^{-\mathrm{i}\omega_n t} + \text{c.c.}$ and $R_n\mathrm{e}^{-\mathrm{i}\omega_n t} + \text{c.c.}$, $n \geqslant 2$) disturbances, and, depending on the flow geometry, the latter may radiate into the far field as secondary reflected beams along specific directions.

We begin by calculating the $O(\epsilon^2)$ induced mean flow. Substituting expansions (3.7) and (3.8) in the governing equations (3.1) and (3.2), collecting $O(\epsilon^2)$ mean terms and making use of the linear solution (3.4), it is found that

$$Q_0 = \frac{\mathrm{i}}{\sin\theta}\, J(Q, Q^*), \tag{3.9a}$$

$$R_0 = \frac{1}{\sin^2\theta}\{\cos\alpha\, J(Q_x, Q^*) - \sin\alpha\, J(Q_y, Q^*)\} + \text{c.c.}. \tag{3.9b}$$

As $J(Q, Q^*)$ is imaginary, Q_0 in (3.9a) is real. Note also that, since the linear solution (3.4) satisfies the boundary condition (3.3) on the slope, Q_0 automatically does so: $Q_{0x} = 0$ on $y = 0$. Moreover, according to (3.9), the induced mean flow remains confined to the region where the incident and reflected beams overlap; away from this interaction region, the Jacobians in (3.9) vanish because the incident and the reflected beams satisfy the full nonlinear governing equations. It should be noted that Q_0 and R_0 are not singular when $\sin\theta = 0$, which corresponds to horizontal incident and reflected beams, because Q vanishes in this case according to (3.5)–(3.6).

Next, we turn to the $O(\epsilon^2)$ second-harmonic and the $O(\epsilon^3)$ third-harmonic terms, as well as the $O(\epsilon^3)$ primary-harmonic corrections, in (3.7) and (3.8). Upon substituting these expansions in (3.1) and (3.2) and collecting terms of equal harmonics, it is found that the amplitudes $Q_n(x, y)$ ($n = 1, 2, 3$) satisfy forced equations of the form

$$(n^2\sin^2\theta - \cos^2\alpha)\, Q_{nxx} + (n^2\sin^2\theta - \sin^2\alpha)\, Q_{nyy} + \sin 2\alpha\, Q_{nxy} = f_n(x, y), \tag{3.10a}$$

subject to the wall boundary condition

$$Q_{nx} = 0 \quad (y = 0); \tag{3.10b}$$

moreover,

$$R_n(x, y) = -\frac{\mathrm{i}}{n\,\sin\theta}(\cos\alpha\, Q_{nx} - \sin\alpha\, Q_{ny}) + h_n(x, y) \qquad (n = 1, 2, 3). \tag{3.11}$$

Explicit expressions for the forcing terms f_n and h_n in (3.10a) and (3.11) are given in Appendix A. Note that these terms are locally confined, as they derive from nonlinear interactions among the incident and reflected beams as well as the induced mean flow.

In addition, the solutions of the forced boundary-value problems (3.10) satisfy suitable conditions at infinity ($y \to \infty$), namely the far-field response is either evanescent or radiates outwards from the slope. More specifically, according to the dispersion relation (2.6), the higher-harmonic corrections can radiate if the corresponding frequency is less than the Brunt–Väisälä frequency, $n\omega < 1$; this in turn places a

https://doi.org/10.1017/S0022112004002769 Published online by Cambridge University Press

restriction on the angle of incidence θ for radiation to be possible:

$$\sin\theta < \frac{1}{n} \qquad (n \geqslant 2); \tag{3.12}$$

otherwise, the higher-harmonic response is evanescent. On the other hand, the correction to the primary harmonic ($n = 1$) can always radiate.

We now proceed to solve the forced problem (3.10) for the correction to the primary harmonic ($n = 1$) and for the second- and third-harmonic responses ($n = 2, 3$) in the case that (3.12) is met so the radiation condition is appropriate far from the sloping wall.

3.1. *Radiating higher harmonics and correction to the primary*

Assuming that (3.12) is satisfied for $n = 2, 3$, it is convenient to introduce the notation

$$\gamma_n = \sin^{-1}(n\sin\theta) \qquad (n = 1, 2, 3), \tag{3.13}$$

γ_1 being the angle of incidence θ.

Returning then to the forced equation (3.10*a*), taking the Fourier transform with respect to x

$$Q_n(x, y) = \int_{-\infty}^{\infty} \hat{Q}_n(l; y)\, \mathrm{e}^{\mathrm{i}lx}\, \mathrm{d}l,$$

and solving the resulting differential equation along y by variation of parameters, $\hat{Q}_n(l; y)$ $(n = 1, 2, 3)$ can be expressed as

$$\begin{aligned}\hat{Q}_n(l; y) = {} & A_n(l)\exp\{\mathrm{i}ly\,\cot(\gamma_n + \alpha)\} + B_n(l)\exp\{-\mathrm{i}ly\,\cot(\gamma_n - \alpha)\} \\ & + \frac{\mathrm{i}}{l\,\sin 2\gamma_n}\left[\exp\{\mathrm{i}ly\,\cot(\gamma_n+\alpha)\}\int_y^{\infty}\exp\{-\mathrm{i}ly'\,\cot(\gamma_n+\alpha)\}\,\hat{f}_n(l, y')\,\mathrm{d}y'\right. \\ & \left. - \exp\{-\mathrm{i}ly\,\cot(\gamma_n-\alpha)\}\int_y^{\infty}\exp\{\mathrm{i}ly'\,\cot(\gamma_n-\alpha)\}\,\hat{f}_n(l, y')\,\mathrm{d}y'\right].\end{aligned} \tag{3.14}$$

The last term in (3.14) accounts for the presence of the forcing $f_n(x, y)$ and is evanescent as $y \to \infty$. The first two terms, on the other hand, correspond to free propagating waves, and the undetermined coefficients $A_n(l)$ and $B_n(l)$ are found by imposing the wall boundary condition (3.10*b*) and the radiation condition noted earlier.

Specifically, for $l > 0$, upon comparison of the two propagating-wave terms in (3.14) against the linear incident and reflected wave beams (3.6*a*) and (3.6*b*), respectively, it is clear that only the second term in (3.14) represents a wave radiating outwards. Hence,

$$A_n(l) = 0 \qquad (l > 0) \tag{3.15a}$$

and, in view of the wall boundary condition (3.10*b*),

$$\begin{aligned}B_n(l) = -\frac{\mathrm{i}}{l\,\sin 2\gamma_n}\int_0^{\infty}\mathrm{d}y'\,\hat{f}_n(l, y')[&\exp\{-\mathrm{i}ly'\,\cot(\gamma_n+\alpha)\} \\ &- \exp\{\mathrm{i}ly'\,\cot(\gamma_n-\alpha)\}].\end{aligned} \tag{3.15b}$$

On the other hand, for $l < 0$, since changing the sign of the wavenumber of a plane wave reverses the direction of the group velocity (see figure 2), only the first term in (3.14) obeys the radiation condition. Hence,

$$B_n(l) = 0 \qquad (l < 0) \tag{3.16a}$$

https://doi.org/10.1017/S0022112004002769 Published online by Cambridge University Press

and, from (3.10*b*),

$$A_n(l) = -\frac{\mathrm{i}}{l \sin 2\gamma_n} \int_0^\infty \mathrm{d}y'\, \hat{f}_n(l, y')[\exp\{-\mathrm{i}ly' \cot(\gamma_n + \alpha)\} - \exp\{\mathrm{i}ly' \cot(\gamma_n - \alpha)\}]. \quad (3.16b)$$

Now, as the linear solution (3.5)–(3.6) involves plane waves with $l > 0$ only, it is straightforward to show from expressions (A 2) and (A 3), that the same is true for the second- and third-harmonic forcing terms f_2 and f_3: $\hat{f}_2(l; y) = \hat{f}_3(l; y) = 0$ for $l < 0$. Therefore, combining (3.14) with (3.15), the radiating portions $Q_n^{\mathrm{refl}}(x, y)$ of the second and third harmonics ($n = 2, 3$) take the form of wave beams that propagate in the far field:

$$Q_n(x, y) \sim Q_n^{\mathrm{refl}}(x, y) = \int_0^\infty \mathrm{d}l\, B_n(l) \exp\{\mathrm{i}\, l(x - y \cot(\gamma_n - \alpha))\} \qquad (y \to \infty), \quad (3.17)$$

where $B_n(l)$ is given by (3.15*b*).

Expression (3.17) for the higher-harmonic reflected beams is entirely analogous to (3.6*b*) for the linear reflected wave beam and can be interpreted along similar lines: the reflected beam of frequency $n\omega\,(= 2, 3)$ propagates at the angle γ_n to the horizontal, deduced from the dispersion relation according to (3.13), and it is found upslope or downslope depending on whether $\gamma_n > \alpha$ or $\gamma_n < \alpha$, respectively. Since the angle of incidence $\theta < \gamma_n$, it is thus possible for higher-harmonic reflected beams to be found on the opposite side to the vertical from the linear reflected beam. Figure 4, in particular, illustrates the various configurations that arise as the slope angle α is varied when the angle of incidence is in the range $\sin^{-1}(1/3) < \theta < \sin^{-1}(1/2)$ so only the second harmonic ($n = 2$) can radiate according to (3.12).

It is clear from (3.17) that $Q_n(x, y)$ is singular when $\gamma_n = \alpha$ so the corresponding higher-harmonic beam is reflected along the slope. This singularity is entirely analogous to the one noted earlier for the primary reflected beam (3.6*b*) when $\theta = \alpha$. Also, according to (3.15*b*) and (3.16*b*), singular behaviour is expected when $\gamma_n = \pi/2$, so the reflected beam propagates vertically. In this instance, a resonance phenomenon occurs owing to the vanishing of the group velocity and no steady state is reached in the absence of viscous effects (Tabaei & Akylas 2003).

Turning next to the primary-harmonic correction, unlike the second and third harmonics, the forcing term $f_1(x, y)$ in equation (3.10*a*) for $Q_1(x, y)$ involves plane waves with both $l > 0$ and $l < 0$ owing to the presence of terms such as $J(R^*, Q_2)$ in expression (A 1). Accordingly, the correction to the primary harmonic impacts both the incident and the reflected primary-harmonic beams. Specifically, from (3.14)–(3.16), recalling that $\gamma_1 = \theta$, the radiating portion of Q_1 in the far field may be written as

$$Q_1(x, y) \sim Q_1^{\mathrm{inc}} + Q_1^{\mathrm{refl}} \qquad (y \to \infty), \quad (3.18)$$

where

$$Q_1^{\mathrm{inc}}(x, y) = \int_{-\infty}^0 \mathrm{d}l\, A_1(l) \exp\{\mathrm{i}\, l(x + y \cot(\theta + \alpha))\} \quad (3.19a)$$

and

$$Q_1^{\mathrm{refl}}(x, y) = \int_0^\infty \mathrm{d}l\, B_1(l) \exp\{\mathrm{i}\, l(x - y \cot(\theta - \alpha))\}, \quad (3.19b)$$

with $A_1(l)$ and $B_1(l)$ given by (3.16*b*) and (3.15*b*), respectively. Expression (3.18) combined with (3.19) is similar to the linear solution (3.5)–(3.6). Q_1^{inc} provides a correction to the incident beam and Q_1^{refl} to the linear reflected beam. As required by the radiation

https://doi.org/10.1017/S0022112004002769 Published online by Cambridge University Press

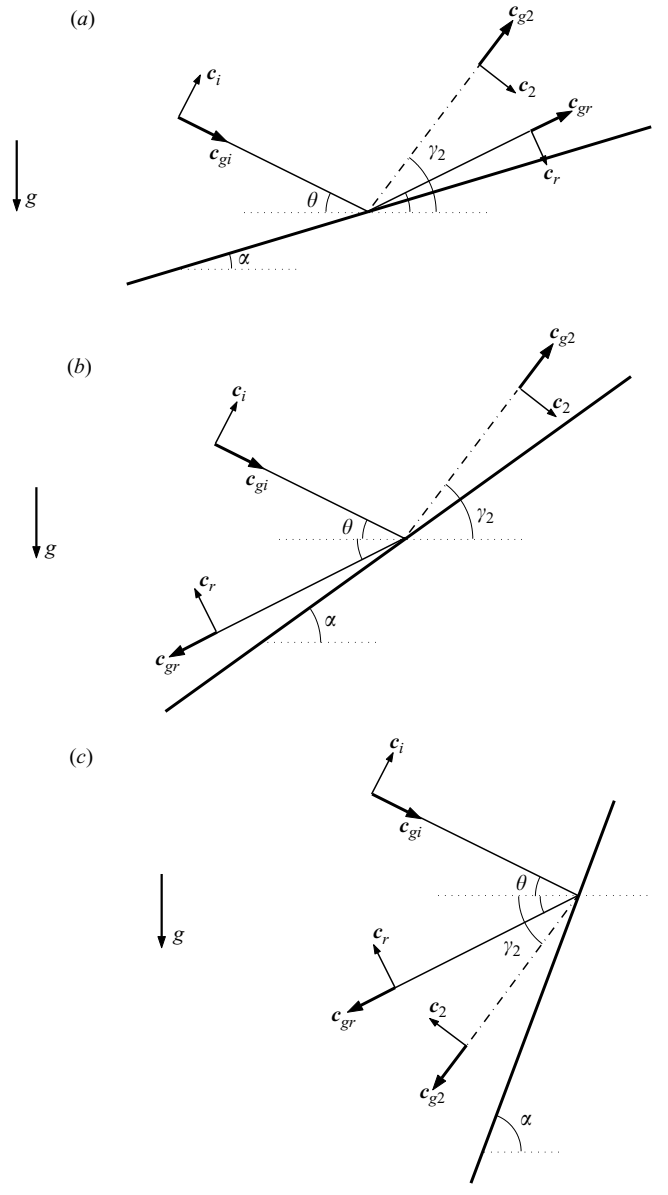

FIGURE 4. Different configurations of incident beam and reflected primary- and second-harmonic beams for a fixed angle of incidence θ and various values of the wall inclination α: (*a*) $\theta > \alpha$, $\gamma_2 > \alpha$; (*b*) $\theta < \alpha$, $\gamma_2 > \alpha$; and (*c*) $\theta < \alpha$, $\gamma_2 < \alpha$. $\boldsymbol{c}_g$ and $\boldsymbol{c}$ are group and phase velocities, respectively; subscripts i, r and 2 denote incident, reflected primary-harmonic and reflected second-harmonic beams, respectively. $\gamma_2 = \sin^{-1}(2\sin\theta)$ denotes the angle of reflection of the second harmonic relative to the horizontal.

condition, both of these corrections radiate outwards from the sloping wall. In the numerical examples discussed in § 6, Q_1^{refl} turns out to be significantly stronger than Q_1^{inc}.

3.2. *Evanescent higher harmonics*

When the angle of incidence θ does not satisfy condition (3.12), the harmonic $n\omega$ is above the Brunt–Väisälä frequency and no radiation is possible. The response then

https://doi.org/10.1017/S0022112004002769 Published online by Cambridge University Press

remains locally confined and the radiation condition is replaced by

$$Q_n(x, y) \to 0 \qquad (y \to \infty). \tag{3.20}$$

In this instance, with the notation $\omega_n = n \sin\theta$, the general solution of the forced equation (3.10a) for the Fourier transform $\hat{Q}_n(l; y)$ reads

$$\begin{aligned}\hat{Q}_n(l; y) = {} & C_n(l) \exp\{(\mathrm{i}a + b)ly\} + D_n(l) \exp\{(\mathrm{i}a - b)ly\} \\ & + \frac{1}{2\omega_n l \sqrt{\omega_n^2 - 1}} \Bigg[\exp\{(\mathrm{i}a - b)ly\} \int_y^\infty \exp\{-(\mathrm{i}a - b)ly'\} \, \hat{f}_n(l, y') \, \mathrm{d}y' \\ & - \exp\{(\mathrm{i}a + b)ly\} \int_y^\infty \exp\{-(\mathrm{i}a + b)ly'\} \, \hat{f}_n(l, y') \, \mathrm{d}y' \Bigg],\end{aligned} \tag{3.21}$$

where

$$a = -\frac{\sin 2\alpha}{2\left(\omega_n^2 - \sin^2\alpha\right)}, \qquad b = \frac{\omega_n \sqrt{\omega_n^2 - 1}}{\omega_n^2 - \sin^2\alpha}.$$

Since $b > 0$, condition (3.20) eliminates $C_n(l)$ for $l > 0$ and $D_n(l)$ for $l < 0$, in the above solution. Moreover, as remarked earlier, $\hat{f}_2(l; y)$ and $\hat{f}_3(l; y)$ are non-zero for $l > 0$ only; hence, $C_n = 0$ and imposing the wall boundary condition (3.10b), determines D_n:

$$D_n(l) = -\frac{1}{\omega_n l \sqrt{\omega_n^2 - 1}} \int_0^\infty \exp(-\mathrm{i}aly') \, \sinh(bly') \, \hat{f}_n(l, y') \, \mathrm{d}y' \qquad (l > 0). \tag{3.22}$$

Finally, combining (3.22) with (3.21), after some manipulation, yields

$$\begin{aligned}\hat{Q}_n(l; y) = {} & \frac{1}{2\omega_n l \sqrt{\omega_n^2 - 1}} \Bigg[\exp\{(\mathrm{i}a - b)ly\} \int_0^\infty \exp\{-(\mathrm{i}a + b)ly'\} \, \hat{f}_n(l, y') \, \mathrm{d}y' \\ & - \int_y^\infty \exp\{-(\mathrm{i}a + b)(y' - y)l\} \, \hat{f}_n(l, y') \, \mathrm{d}y' \\ & - \int_0^y \exp\{(\mathrm{i}a - b)(y - y')l\} \, \hat{f}_n(l, y') \, \mathrm{d}y' \Bigg] \quad (l > 0),\end{aligned} \tag{3.23a}$$

$$\hat{Q}_n(l; y) = 0 \quad (l < 0). \tag{3.23b}$$

Note that only exponentially decaying terms in y are present in expression (3.23a), which makes it particularly suitable for computing $\hat{Q}_n(l; y)$. Having determined $\hat{Q}_n(l; y)$, the response amplitude $Q_n(x, y)$ is readily found by inverting the Fourier transform:

$$Q_n(x, y) = \int_0^\infty \hat{Q}_n(l; y) \, \mathrm{e}^{\mathrm{i}lx} \, \mathrm{d}l. \tag{3.24}$$

4. Energy partition

As noted in § 2, in general, there is non-zero energy flux in the direction of propagation of a wave beam. Accordingly, in the reflection of a wave beam from a sloping wall, it is of interest to ask how the incident energy flow rate is partitioned among the reflected wave beams.

Based on the conservation law (2.11), the average energy flow rate entering a fixed control volume is equal to the average energy flow rate leaving this volume. Hence,

https://doi.org/10.1017/S0022112004002769 Published online by Cambridge University Press

in the problem at hand, considering a large control volume bounded by the sloping wall ($y=0$) and $y=y_\infty$, where y_∞ is taken to lie in the far field ($y_\infty \gg 1$), the energy flow rate in the incident beam must exactly balance the total energy flow rate in the reflected wave beams. Moreover, as these beams are well separated in the far field, it is legitimate to use expression (2.12), derived for a single uniform beam, in order to compute the corresponding energy flow rates.

For the incident beam, in particular, the amplitude profile, correct to $O(\epsilon^3)$, is given by $\epsilon Q^{\mathrm{inc}} + \epsilon^3 Q_1^{\mathrm{inc}}$, Q^{inc} being the amplitude of the incident beam in (3.6*a*) and Q_1^{inc} the correction (3.19*a*) induced by nonlinear interactions. Making use of (2.12), the average incoming energy flow rate, correct to $O(\epsilon^4)$, then can be expressed as

$$\mathscr{F}^{\mathrm{inc}} = 2\mathrm{i}\epsilon^2 \cos\theta \left\{ \int_{-\infty}^{\infty} Q^{\mathrm{inc}^*} Q_\eta^{\mathrm{inc}} \,\mathrm{d}\eta - \epsilon^2 \int_{-\infty}^{\infty} \left(Q_\eta^{\mathrm{inc}^*} Q_1^{\mathrm{inc}} - \mathrm{c.c.} \right) \mathrm{d}\eta \right\}.$$

However, from the fact that Q^{inc} and Q_1^{inc} transport energy in opposite directions – they comprise plane waves with opposite wavenumbers according to (3.6*a*) and (3.19*a*) – it follows that the $O(\epsilon^4)$ integrals above vanish. Hence, correct to $O(\epsilon^4)$,

$$\mathscr{F}^{\mathrm{inc}} = 2\mathrm{i}\epsilon^2 \cos\theta \int_{-\infty}^{\infty} Q^{\mathrm{inc}^*} Q_\eta^{\mathrm{inc}} \,\mathrm{d}\eta. \tag{4.1}$$

Similarly, combining (2.12), (3.6*b*) and (3.19*b*), the outgoing energy flow rate, correct to $O(\epsilon^4)$, for the reflected first-harmonic beam is found to be

$$\mathscr{F}_1^{\mathrm{refl}} = -2\mathrm{i}\epsilon^2 \cos\theta \left\{ \int_{-\infty}^{\infty} Q^{\mathrm{refl}^*} Q_\eta^{\mathrm{refl}} \,\mathrm{d}\eta - \epsilon^2 \int_{-\infty}^{\infty} \left(Q_\eta^{\mathrm{refl}^*} Q_1^{\mathrm{refl}} - \mathrm{c.c.} \right) \mathrm{d}\eta \right\}. \tag{4.2}$$

Note that the $O(\epsilon^4)$ integrals in the above expression in general are non-zero since Q^{refl} and Q_1^{refl} transport energy in the same direction.

Finally, if the second harmonic radiates, inserting (3.17) for $n=2$ in (2.12), it is found that the corresponding outgoing energy flow rate is

$$\mathscr{F}_2^{\mathrm{refl}} = -2\mathrm{i}\epsilon^4 \cos\gamma_2 \int_{-\infty}^{\infty} Q^{\mathrm{refl}^*} Q_{2\eta}^{\mathrm{refl}} \,\mathrm{d}\eta. \tag{4.3}$$

Now, as remarked earlier, it follows from conservation of energy that the net average energy flow rate entering and leaving a control volume must vanish. Hence, combining (4.1)–(4.3),

$$\mathscr{F}^{\mathrm{inc}} + \mathscr{F}_1^{\mathrm{refl}} + \mathscr{F}_2^{\mathrm{refl}} = 0. \tag{4.4}$$

As expected, the $O(\epsilon^2)$ terms in (4.1) and (4.2) cancel out in view of the fact that the linear solution (3.4)–(3.6) is consistent with energy conservation, thus leaving only $O(\epsilon^4)$ terms in the energy balance equation (4.4):

$$2\cos\theta \int_{-\infty}^{\infty} \mathrm{Im}\{ Q_x^{\mathrm{refl}^*} Q_1^{\mathrm{refl}} \} \,\mathrm{d}x + \mathrm{i}\cos\gamma_2 \int_{-\infty}^{\infty} Q_2^{\mathrm{refl}^*} Q_{2x}^{\mathrm{refl}} \,\mathrm{d}x = 0, \tag{4.5}$$

where $\mathrm{Im}\{.\}$ stands for the imaginary part and with the understanding that the second term is absent if the second harmonic happens to be evanescent. Also, it should be noted that the cross-beam variable η used in (4.1)–(4.3) has been replaced by x in (4.5) since the energy flow rate in a beam can be calculated by integrating along any direction across the beam.

https://doi.org/10.1017/S0022112004002769 Published online by Cambridge University Press

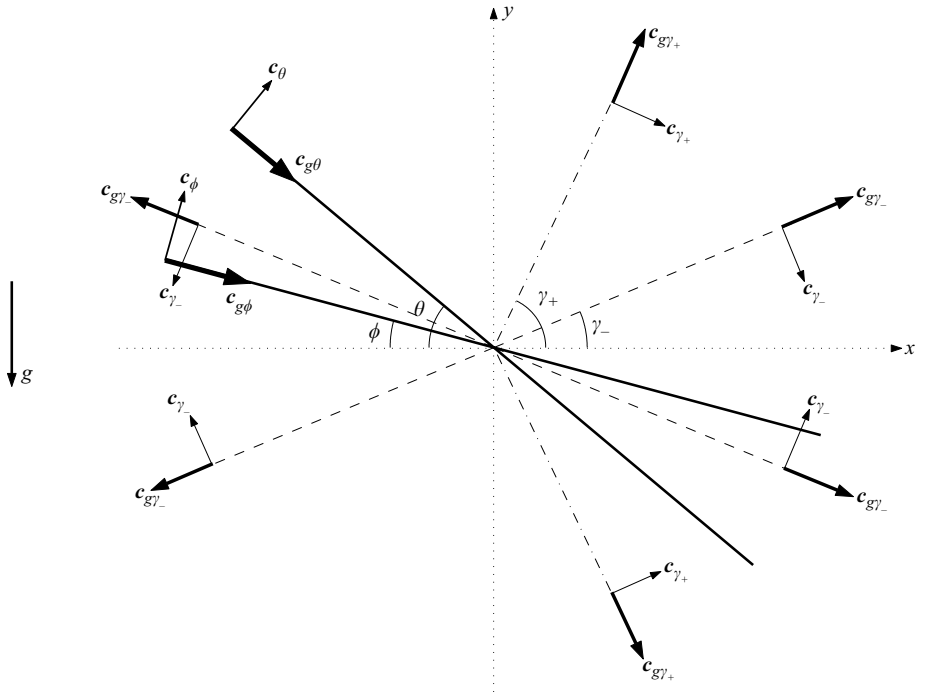

FIGURE 5. Two uniform wave beams approaching each other at angles θ and ϕ to the horizontal ($0 < \phi < \theta < \pi/2$). Additional beams with frequency $\omega_\theta - \omega_\phi$ (— —) and $\omega_\theta + \omega_\phi$ (–·–) are induced by quadratic nonlinear interactions in the collision region of the two primary beams.

5. Colliding wave beams

We now turn to a discussion of nonlinear effects in collisions of wave beams. To be specific, we shall take two beams approaching each other at angles θ and ϕ to the horizontal and focus attention on the particular configuration $0 < \phi < \theta < \pi/2$ shown in figure 5. (Results for other configurations are summarized later in § 5.1.) According to the dispersion relation (2.6), the corresponding frequencies are $\omega_\theta = \sin\theta$ and $\omega_\phi = \sin\phi$ with $\omega_\theta > \omega_\phi > 0$. Moreover, in the present setting, there is no need to rotate axes so we revert to the original coordinates, x and y denoting the horizontal and vertical direction, respectively, and place the origin within the interaction region of the two beams (see figure 5).

Following the same approach as before, assuming that the beams are weakly nonlinear, ψ is expanded in terms of an amplitude parameter $\epsilon \ll 1$:

$$\begin{aligned}\psi = {} & \epsilon\{(Q^\theta(x,y)\,\mathrm{e}^{-\mathrm{i}\omega_\theta t} + \text{c.c.}) + (Q^\phi(x,y)\,\mathrm{e}^{-\mathrm{i}\omega_\phi t} + \text{c.c.})\} \\ & + \epsilon^2\{(Q^{\theta+\phi}(x,y)\,\mathrm{e}^{-\mathrm{i}(\omega_\theta+\omega_\phi)t} + \text{c.c.}) + (Q^{\theta-\phi}(x,y)\,\mathrm{e}^{-\mathrm{i}(\omega_\theta-\omega_\phi)t} + \text{c.c.})\} \\ & + \epsilon^3\{(Q_1^\theta(x,y)\,\mathrm{e}^{-\mathrm{i}\omega_\theta t} + \text{c.c.}) + (Q_1^\phi(x,y)\,\mathrm{e}^{-\mathrm{i}\omega_\phi t} + \text{c.c.})\} \\ & + \epsilon^3\{(Q^{2\theta+\phi}(x,y)\,\mathrm{e}^{-\mathrm{i}(2\omega_\theta+\omega_\phi)t} + \text{c.c.}) + (Q^{2\theta-\phi}(x,y)\,\mathrm{e}^{-\mathrm{i}(2\omega_\theta-\omega_\phi)t} + \text{c.c.}) \\ & + (Q^{\theta+2\phi}(x,y)\,\mathrm{e}^{-\mathrm{i}(\omega_\theta+2\omega_\phi)t} + \text{c.c.}) + (Q^{\theta-2\phi}(x,y)\,\mathrm{e}^{-\mathrm{i}(\omega_\theta-2\omega_\phi)t} + \text{c.c.})\} + \cdots, \end{aligned} \tag{5.1}$$

https://doi.org/10.1017/S0022112004002769 Published online by Cambridge University Press

with a similar expansion for ρ in which Q^{θ}, $Q^{\phi}, \ldots, Q^{\theta-2\phi}$ are replaced with R^{θ}, $R^{\phi}, \ldots, R^{\theta-2\phi}$, respectively. The leading-order terms in these expansions,

$$Q^{\theta(\phi)}(x, y) = \int_0^{\infty} A^{\theta(\phi)}(l)\, \exp\{\mathrm{i}l(x + y\cot\theta(\phi))\}\mathrm{d}l, \tag{5.2a}$$

$$R^{\theta(\phi)}(x, y) = -\frac{\mathrm{i}}{\omega_{\theta(\phi)}} Q_x^{\theta(\phi)}, \tag{5.2b}$$

correspond to two uniform beams of the form (2.7) and (2.8) going through each other without any interaction, in accordance with the linear theory. Both beams involve plane waves with positive horizontal and vertical wavenumber components so that the group velocities (see figure 2), and hence the beam directions, are consistent with those in figure 5. As in (2.9), the spectral amplitudes A^{θ} and A^{ϕ} are related to the Fourier transform of the cross-sectional profile of each beam.

The higher-order terms in expansion (5.1) anticipate additional harmonics involving sums and differences of the beam frequencies ω_{θ} and ω_{ϕ}, owing to nonlinear interactions in the region where the two beams overlap. Based on previous experience, those harmonics that are below the Brunt–Väisälä frequency are expected to result in additional beams propagating outwards from this interaction region. On the other hand, no mean, second and third harmonics of ω_{θ} and ω_{ϕ} are present in expansion (5.1) up to $O(\epsilon^3)$, since each of the colliding beams is an exact nonlinear solution and all self-interaction nonlinear terms vanish.

5.1. $O(\epsilon^2)$ *response*

Proceeding next to $O(\epsilon^2)$, upon substitution of (5.1) into the governing equations (2.4) and (2.5), collecting terms involving the harmonics $\Omega_{\pm} \equiv \omega_{\theta} \pm \omega_{\phi}$, it is found that the amplitudes $Q^{\pm} \equiv Q^{\theta\pm\phi}$ satisfy forced equations of the form

$$\Omega_{\pm}^2\, Q_{yy}^{\pm} - (1 - \Omega_{\pm}^2)\, Q_{xx}^{\pm} = \mathfrak{R}^{\pm}(x, y), \tag{5.3}$$

where

$$\mathfrak{R}^{+} = \mathrm{i}\frac{\Omega_-}{\omega_{\theta}\omega_{\phi}} J\left(Q_x^{\theta}, Q_x^{\phi}\right) - \mathrm{i}\frac{\Omega_+ + \omega_{\theta}}{\omega_{\theta}^2} J\left(Q_{xx}^{\theta}, Q^{\phi}\right) - \mathrm{i}\frac{\Omega_+ + \omega_{\phi}}{\omega_{\phi}^2} J\left(Q_{xx}^{\phi}, Q^{\theta}\right), \tag{5.4a}$$

$$\mathfrak{R}^{-} = -\mathrm{i}\frac{\Omega_+}{\omega_{\theta}\omega_{\phi}} J\left(Q_x^{\theta}, Q_x^{\phi^*}\right) - \mathrm{i}\frac{\Omega_- + \omega_{\theta}}{\omega_{\theta}^2} J\left(Q_{xx}^{\theta}, Q^{\phi^*}\right) - \mathrm{i}\frac{\Omega_- - \omega_{\phi}}{\omega_{\phi}^2} J\left(Q_{xx}^{\phi\,*}, Q^{\theta}\right). \tag{5.4b}$$

Also the corresponding amplitudes $R^{\pm} \equiv R^{\theta\pm\phi}$ in the expansion of the density perturbation ρ, analogous to (5.1), are given by

$$R^{+} = -\frac{\mathrm{i}}{\Omega_+} Q_x^{+} - \frac{1}{\omega_{\theta}\Omega_+} J\left(Q_x^{\theta}, Q^{\phi}\right) - \frac{1}{\omega_{\phi}\Omega_+} J\left(Q_x^{\phi}, Q^{\theta}\right), \tag{5.5a}$$

$$R^{-} = -\frac{\mathrm{i}}{\Omega_-} Q_x^{-} - \frac{1}{\omega_{\theta}\Omega_-} J\left(Q_x^{\theta}, Q^{\phi^*}\right) + \frac{1}{\omega_{\phi}\Omega_-} J\left(Q_x^{\phi^*}, Q^{\theta}\right). \tag{5.5b}$$

The forcing terms (5.4) are locally confined in the interaction region of the two colliding beams. The far-field behaviour of $Q^{\pm}(x, y)$, on the other hand, hinges on whether the harmonics $\Omega_{\pm}$ are below or above 1 (the normalized Brunt–Väisälä frequency), the $O(\epsilon^2)$ response radiating additional wave beams when $\Omega_{\pm} < 1$ or being locally confined otherwise.

Specifically, assuming that $\Omega_+ < 1$, it is convenient to introduce

$$\gamma_+ = \sin^{-1}\Omega_+, \tag{5.6}$$

https://doi.org/10.1017/S0022112004002769 Published online by Cambridge University Press

and upon taking the Fourier transform in x,

$$Q^+(x,y)=\int_{-\infty}^{\infty}\hat{Q}^+(l;y)\,\mathrm{e}^{\mathrm{i}lx}\,\mathrm{d}l,$$

equation (5.3) yields

$$\sin^2\gamma_+\,\hat{Q}^+_{yy}+l^2\cos^2\gamma_+\,\hat{Q}^+=\hat{\mathfrak{R}}^+(l;y). \tag{5.7}$$

According to (5.2a), $\hat{Q}^{\theta(\phi)}(l;y)=0$ for $l<0$ so, from (5.4a), $\hat{\mathfrak{R}}^+(l;y)=0$ for $l<0$ as well. In solving (5.7), therefore, we need only consider $l>0$, in which case (see figure 2) $\hat{Q}^+(l;y)$ must obey the following radiation conditions

$$\hat{Q}^+(l;y)\sim\exp\{\mp\mathrm{i}ly\cot\gamma_+\}\qquad(y\to\pm\infty). \tag{5.8}$$

The solution of (5.7) consistent with (5.8) is readily obtained by variation of parameters, and upon inverting the Fourier transform, the response amplitude $Q^+(x,y)$ is found to be

$$\begin{aligned}Q^+(x,y)=\mathrm{i}\int_0^{\infty}\mathrm{d}l\exp\{\mathrm{i}l(x-y\cot\gamma_+)\}\int_{-\infty}^{y}\frac{\hat{\mathfrak{R}}^+(l;y')}{l\sin2\gamma_+}\mathrm{e}^{\mathrm{i}ly'\cot\gamma_+}\,\mathrm{d}y'\\+\mathrm{i}\int_0^{\infty}\mathrm{d}l\exp\{\mathrm{i}l(x+y\cot\gamma_+)\}\int_{y}^{\infty}\frac{\hat{\mathfrak{R}}^+(l;y')}{l\sin2\gamma_+}\mathrm{e}^{-\mathrm{i}ly'\cot\gamma_+}\,\mathrm{d}y'.\end{aligned} \tag{5.9}$$

Far from the interaction region of the colliding beams, the two terms in the above expression describe uniform beams propagating in $x>0$ and inclined symmetrically to the horizontal at the angle γ_+ (see figure 5).

On the other hand, if $\Omega_+>1$, equation (5.3) is elliptic and does not support wave propagation. The radiation conditions (5.8) are then replaced with

$$\hat{Q}^+(l;y)\sim\exp\left\{\mp ly\frac{(\Omega_+^2-1)^{1/2}}{\Omega_+}\right\}\qquad(y\to\pm\infty), \tag{5.10}$$

and, following the same solution procedure as before, it is straightforward to determine the response amplitude $Q^+(x,y)$ which now remains locally confined.

Turning next to $Q^-(x,y)$, the corresponding frequency is in the range $0<\Omega_-<1$ so, according to the dispersion relation (2.6), this harmonic is expected to radiate wave beams inclined at the angle

$$\gamma_-=\sin^{-1}\Omega_- \tag{5.11}$$

relative to the horizontal. Solving then the forced equation (5.3) by taking the Fourier transform in x,

$$\sin^2\gamma_-\,\hat{Q}^-_{yy}+l^2\cos^2\gamma_-\,\hat{Q}^-=\hat{\mathfrak{R}}^-(l;y), \tag{5.12}$$

we remark that both $l>0$ and $l<0$ make a contribution, since $\mathfrak{R}^-(x,y)$ in (5.4b) involves $Q^{\theta(\phi)}$ and $Q^{\theta(\phi)^*}$ so $\hat{\mathfrak{R}}^-(l;y)$ is not zero for $l<0$. Moreover, from figure 2, we infer that $\hat{Q}^-(l;y)$ must adhere to the following radiation conditions

$$\hat{Q}^-(l;y)\sim\exp\{\mp\mathrm{i}|l|y\cot\gamma_-\}\qquad(y\to\pm\infty). \tag{5.13}$$

https://doi.org/10.1017/S0022112004002769 Published online by Cambridge University Press

Angle of incidence θ	Number of induced beams with frequency $\lvert\Omega_+\rvert \equiv \lvert\omega_\theta + \omega_\phi\rvert \neq 0$	Number of induced beams with frequency $\lvert\Omega_-\rvert \equiv \lvert\omega_\theta - \omega_\phi\rvert \neq 0$
$0 < \theta < \pi/2$ $(0 < \omega_\theta < 1)$	2 if $\Omega_+ < 1$ (figure 6*a*) 0 if $\Omega_+ > 1$	4 (figure 7*a*)
$\pi/2 < \theta < \pi$ $(0 < \omega_\theta < 1)$	4 if $\Omega_+ < 1$ (figure 6*b*) 0 if $\Omega_+ > 1$	2 (figure 7*b* if $\Omega_- > 0$; figure 7*c* if $\Omega_- < 0$)
$\pi < \theta < 3\pi/2$ $(-1 < \omega_\theta < 0)$	2 (figure 6*c* if $\Omega_+ < 0$; figure 6*d* if $\Omega_+ > 0$)	4 if $\lvert\Omega_-\rvert < 1$ (figure 7*d*) 0 if $\lvert\Omega_-\rvert > 1$
$3\pi/2 < \theta < 2\pi$ $(-1 < \omega_\theta < 0)$	4 (figure 6*e*)	2 if $\lvert\Omega_-\rvert < 1$ (figure 7*e*) 0 if $\lvert\Omega_-\rvert > 1$

TABLE 1. Number of beams generated by quadratic nonlinear interactions for different configurations of colliding beams approaching each other at angles θ and ϕ to the horizontal, $0 < \phi < \pi/2$ $(0 < \omega_\phi < 1)$.

As before, the solution of equation (5.12) subject to these far-field conditions is found by variation of parameters and, upon inverting the Fourier transform,

$$\begin{aligned} Q^-(x,y) = {} & \mathrm{i}\int_0^\infty \mathrm{d}l\,\exp\{\mathrm{i}l(x - y\cot\gamma_-)\}\int_{-\infty}^{y}\frac{\hat{\mathfrak{R}}^-(l;y')}{l\sin 2\gamma_-}\,\mathrm{e}^{\mathrm{i}ly'\cot\gamma_-}\,\mathrm{d}y' \\ & -\mathrm{i}\int_{-\infty}^0 \mathrm{d}l\,\exp\{\mathrm{i}l(x + y\cot\gamma_-)\}\int_{-\infty}^{y}\frac{\hat{\mathfrak{R}}^-(l;y')}{l\sin 2\gamma_-}\,\mathrm{e}^{-\mathrm{i}ly'\cot\gamma_-}\,\mathrm{d}y' \\ & -\mathrm{i}\int_{-\infty}^0 \mathrm{d}l\,\exp\{\mathrm{i}l(x - y\cot\gamma_-)\}\int_{y}^{\infty}\frac{\hat{\mathfrak{R}}^-(l;y')}{l\sin 2\gamma_-}\,\mathrm{e}^{\mathrm{i}ly'\cot\gamma_-}\,\mathrm{d}y' \\ & +\mathrm{i}\int_0^\infty \mathrm{d}l\,\exp\{\mathrm{i}l(x + y\cot\gamma_-)\}\int_{y}^{\infty}\frac{\hat{\mathfrak{R}}^-(l;y')}{l\sin 2\gamma_-}\,\mathrm{e}^{-\mathrm{i}ly'\cot\gamma_-}\,\mathrm{d}y'. \end{aligned} \tag{5.14}$$

Far from the interaction region, the response (5.14) comprises four wave beams propagating outwards along the directions $\pm\gamma_-$ to the horizontal (see figure 5). This wave geometry is akin to the classical wave pattern, also known as 'St Andrew's Cross', which is generated by a time-harmonic source, such as an oscillating cylinder, in a uniformly stratified Boussinesq fluid (Lighthill 1978, §4.4). Here, however, the four arms of the cross are not equally strong since the interaction region of the two beams, which acts as the source, is not symmetric in general.

Based on (5.9) and (5.14), we conclude that quadratic nonlinear interactions in collisions of two wave beams with frequencies $\omega_\theta > \omega_\phi > 0$ (see figure 5) can induce up to six additional beams: four beams with frequency $\Omega_- = \omega_\theta - \omega_\phi$ forming a St Andrew's Cross, and possibly two beams with frequency $\Omega_+ = \omega_\theta + \omega_\phi$ if $\Omega_+ < 1$.

The secondary beams resulting from quadratic interactions in other configurations of colliding beams can be obtained along similar lines, and the results are summarized in figures 6 and 7 and in table 1. Note that the singular behaviour suggested by the presence of $\Omega_\pm$ in the denominator of expression (5.5*a*,*b*) for $R^\pm$ is only apparent. When the two colliding beams approach each other at the same angle to the horizontal so $\Omega_\pm = 0$ $(\omega_\theta = \mp\omega_\phi)$, $Q^\pm(x, y)$ corresponds to a mean-flow component that is readily found from (5.3) and remains locally confined; moreover, $R^\pm$ is not singular because it turns out that the numerator of (5.5*a*,*b*) vanishes as well when $\Omega_\pm = 0$.

https://doi.org/10.1017/S0022112004002769 Published online by Cambridge University Press

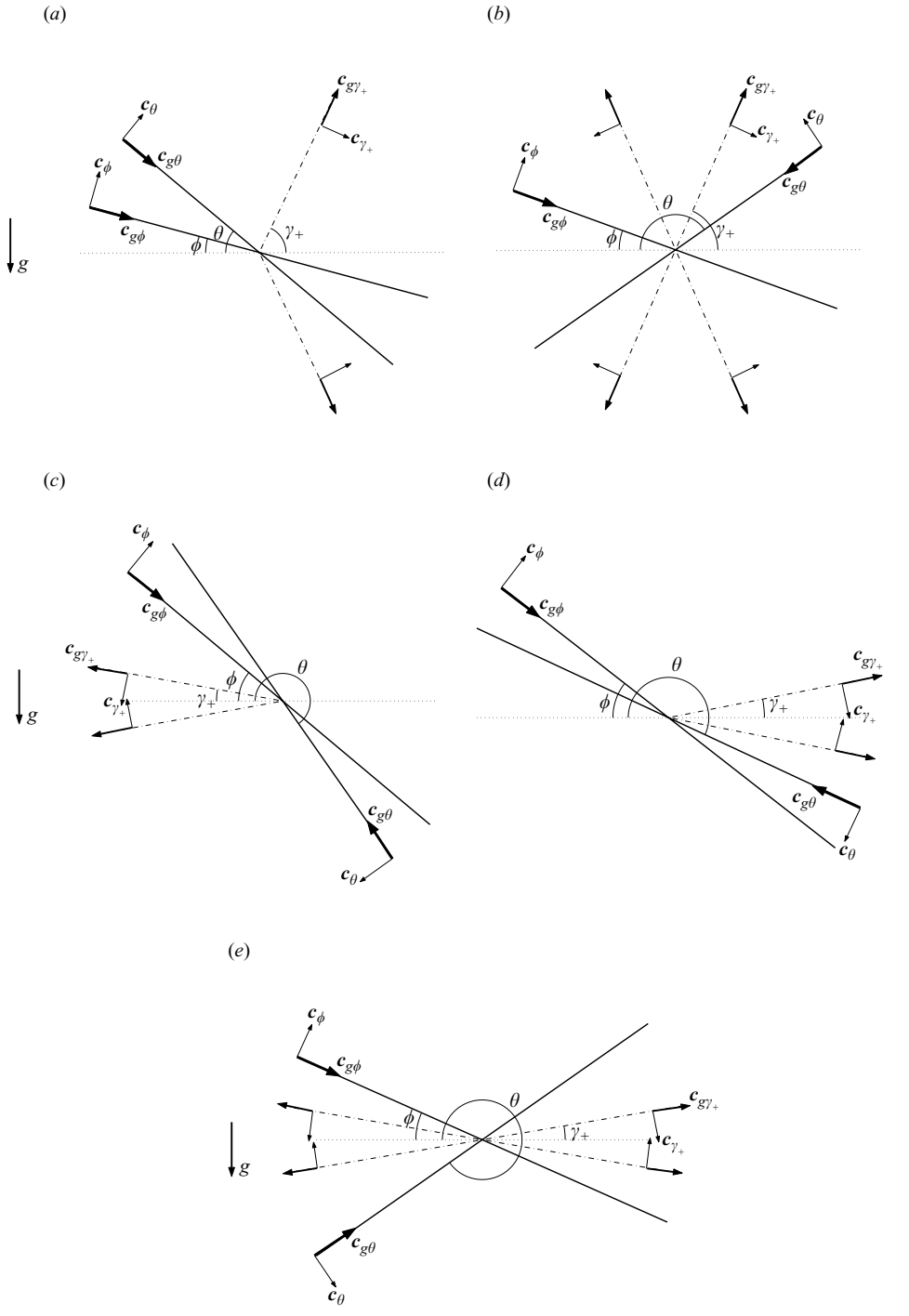

FIGURE 6. Different configurations of colliding beams (—) approaching each other at angles θ and ϕ to the horizontal, and secondary beams (–·–) with frequency $|\Omega_+| \equiv |\omega_\theta + \omega_\phi| \neq 0$ resulting from quadratic interactions. The angle ϕ is in the range $0 < \phi < \pi/2$ and θ varies: (*a*) $0 < \theta < \pi/2$; (*b*) $\pi/2 < \theta < \pi$; (*c*) $\pi < \theta < 3\pi/2$ with $\Omega_+ < 0$; (*d*) $\pi < \theta < 3\pi/2$ with $\Omega_+ > 0$; and (*e*) $3\pi/2 < \theta < 2\pi$.

https://doi.org/10.1017/S0022112004002769 Published online by Cambridge University Press

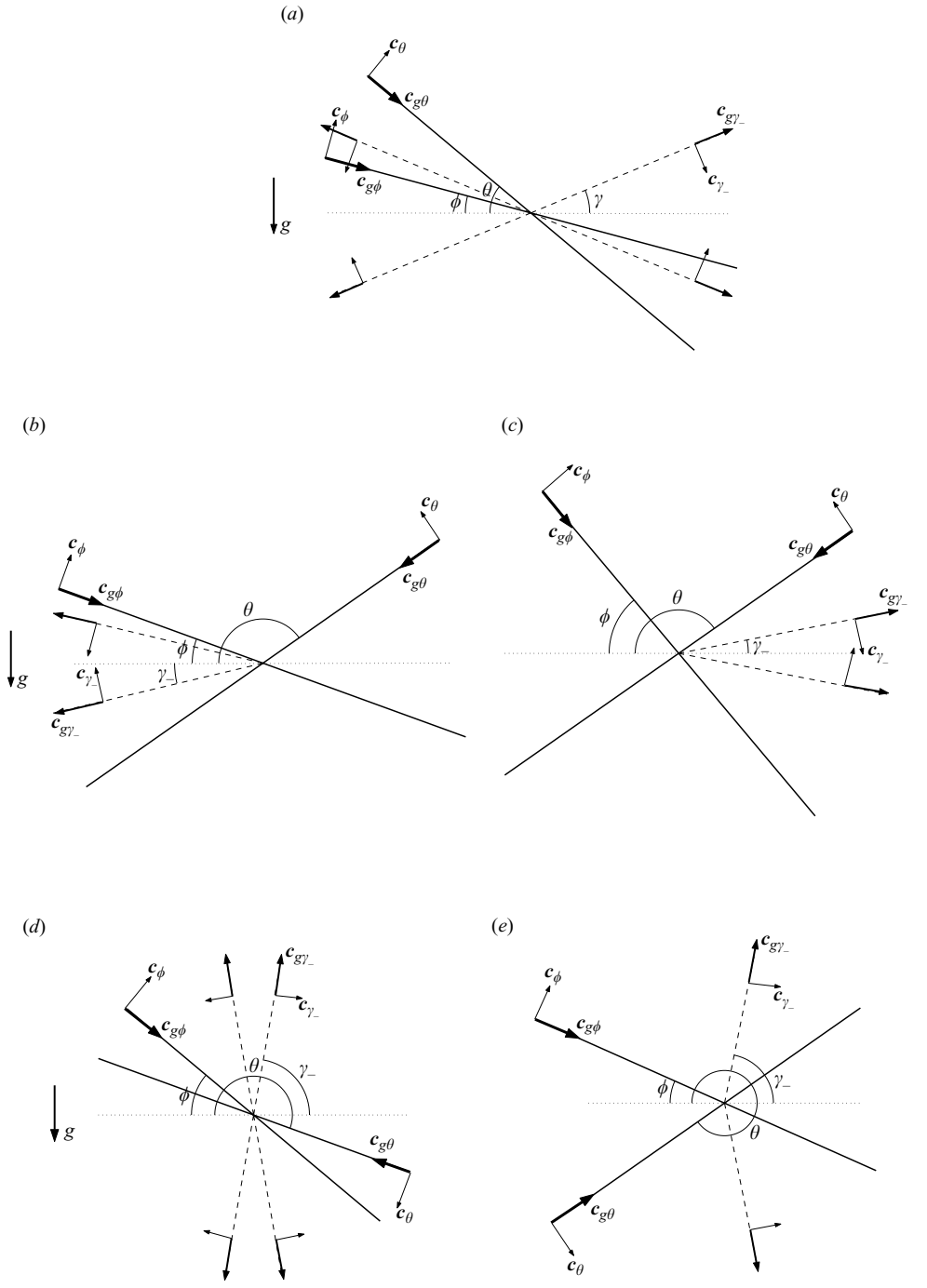

FIGURE 7. Different configurations of colliding beams (—) approaching each other at angles θ and ϕ to the horizontal, and secondary beams (– –) with frequency $|\Omega_-| \equiv |\omega_\theta - \omega_\phi| \neq 0$ resulting from quadratic interactions. The angle ϕ is in the range $0 < \phi < \pi/2$ and θ varies: (*a*) $0 < \theta < \pi/2$; (*b*) $\pi/2 < \theta < \pi$ with $\Omega_- > 0$; (*c*) $\pi/2 < \theta < \pi$ with $\Omega_- < 0$; (*d*) $\pi < \theta < 3\pi/2$; and (*e*) $3\pi/2 < \theta < 2\pi$.

https://doi.org/10.1017/S0022112004002769 Published online by Cambridge University Press

5.2. $O(\epsilon^3)$ response

As anticipated in expansion (5.1), cubic nonlinear interactions give rise to $O(\epsilon^3)$ disturbances with frequencies ω_θ and ω_ϕ as well as additional harmonics. Specifically, the corrections to the primary harmonics satisfy the forced problems

$$\omega_{\theta(\phi)}^2\, Q_{1yy}^{\theta(\phi)} - \left(1-\omega_{\theta(\phi)}^2\right) Q_{1xx}^{\theta(\phi)} = \mathfrak{R}_1^{\theta(\phi)} \tag{5.15}$$

with

$$\mathfrak{R}_1^{\theta} = \{J(R^{\phi}, Q^{-}) + J(R^{\phi^*}, Q^{+}) + J(R^{-}, Q^{\phi}) + J(R^{+}, Q^{\phi^*})\}_x$$
$$- \mathrm{i}\omega_\theta\{J(\nabla^2 Q^{\phi}, Q^{-}) + J(\nabla^2 Q^{\phi^*}, Q^{+}) + J(\nabla^2 Q^{-}, Q^{\phi}) + J(\nabla^2 Q^{+}, Q^{\phi^*})\}, \tag{5.16a}$$

$$\mathfrak{R}_1^{\phi} = \{J(R^{\theta}, Q^{-^*}) + J(R^{\theta^*}, Q^{+}) + J(R^{-^*}, Q^{\theta}) + J(R^{+}, Q^{\theta^*})\}_x$$
$$- \mathrm{i}\omega_\phi\{J(\nabla^2 Q^{\theta}, Q^{-^*}) + J(\nabla^2 Q^{\theta^*}, Q^{+}) + J(\nabla^2 Q^{-^*}, Q^{\theta}) + J(\nabla^2 Q^{+}, Q^{\theta^*})\}. \tag{5.16b}$$

The procedure for solving these problems parallels that used for Q^- in § 5.1. Taking the Fourier transform in x as before, the forcing terms (5.16) involve plane waves with both positive and negative wavenumbers, and the response $Q^{\theta(\phi)}(x, y)$ takes the form of a full St Andrew's Cross with four arms, of not equal strength in general, inclined at the angles $\pm\theta(\phi)$ to the horizontal. Consistent with the radiation condition, all the beams radiate outwards from the interaction region; those, in particular, propagating along θ and ϕ slightly modify the energy flow rate in the primary colliding beams and impact the energy-balance equation at $O(\epsilon^4)$. The rest of the harmonics generated at $O(\epsilon^3)$ have no bearing on energy balance correct to $O(\epsilon^4)$. (The forced problems satisfied by these harmonics are summarized in Appendix B.)

6. Numerical results

Based on the preceding analysis, the region where two internal wave beams meet, owing to nonlinear interactions there, acts as a localized source of additional harmonics that may propagate as secondary beams in the far field. Invoking the appropriate radiation condition, we determined the various steady-state patterns of wave beams, correct to third order in the amplitude parameter ϵ, that arise in the reflection of a beam from a uniform slope and in oblique collisions of two beams. In general, the new beams appearing at each order of the perturbation expansion, are not equally prominent; the profiles of the primary beams, the flow geometry and the nonlinear parameter ϵ are three factors that play an important part in determining the strength of each of these higher-order beams, and hence the overall appearance of the response.

Here, we illustrate the predictions of the perturbation analysis by computing the induced weakly nonlinear wave patterns, correct to $O(\epsilon^3)$, for a few specific examples of reflections and collisions of uniform beams. In these calculations, the incident primary beams are assumed to have a Gaussian profile, such that

$$\psi(\eta, t=0) = \epsilon \exp(-2\eta^2) \tag{6.1}$$

for each beam, η being the cross-beam coordinate. The amplitude parameter ϵ was set to $\epsilon = 0.02$ for the beam reflections in § 6.1 and $\epsilon = 0.05$ for the beam collisions in § 6.2.

We also present one example of beam reflection obtained from unsteady numerical simulations of the full equations of motion. These results confirm the validity of the radiation condition used in the steady-state analysis.

https://doi.org/10.1017/S0022112004002769 Published online by Cambridge University Press

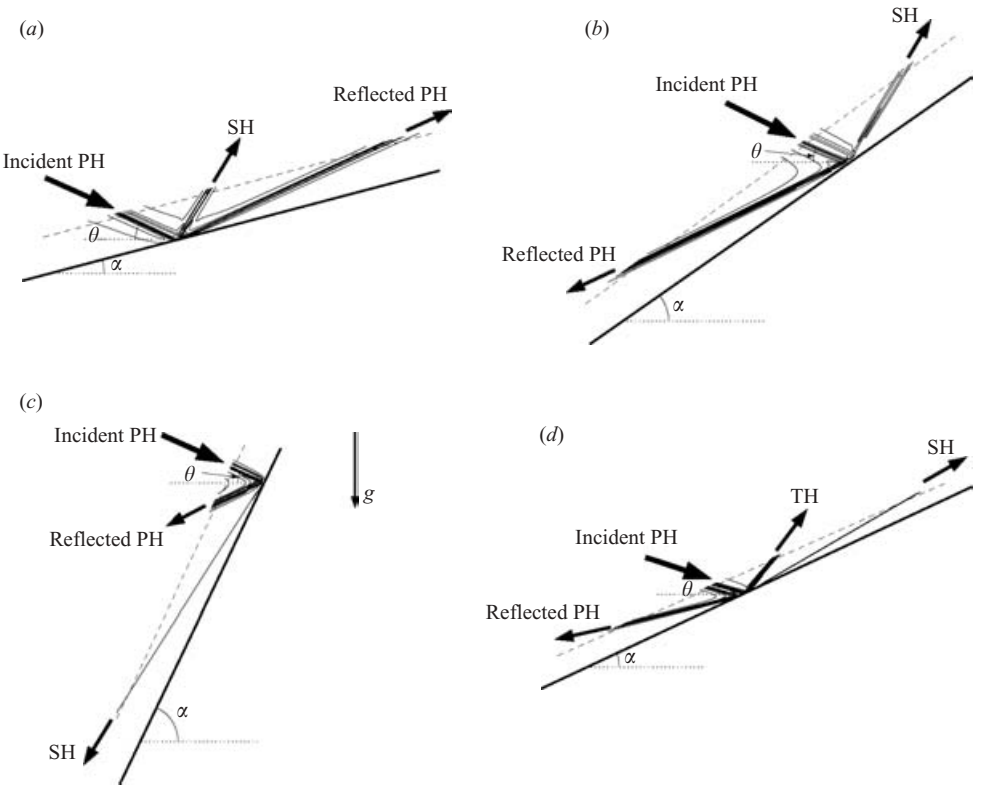

FIGURE 8. Contour plots of the streamfunction ψ at $t = 10$ for different configurations of reflection of an incident wave beam from a slope: (*a*) slope inclination $\alpha = 15°$; (*b*) $\alpha = 35°$; (*c*) $\alpha = 65°$; (*d*) $\alpha = 25°$. (*a–c*) Angle of incidence $\theta = 25°$, $\sin^{-1}(1/3) < \theta < \sin^{-1}(1/2)$ so only the second harmonic can radiate, corresponding to the three configurations shown in figure 4; (*d*) $\theta = 15°$, $\sin^{-1}(1/4) < \theta < \sin^{-1}(1/3)$ so the third harmonic can radiate as well. PH, SH, and TH stand for the primary, second and third harmonic, respectively. Dashed lines (--) indicate the cross-sections of these plots shown in figure 9(*a–d*).

6.1. *Reflection from a slope*

Figure 8 displays contour plots of the streamfunction ψ at $t = 10$, computed from (3.7) correct to $O(\epsilon^3)$, for four cases of reflection of a wave beam from a slope. In figure 8(*a–c*), the angle of incidence $\theta = 25°$ is fixed; since $\sin^{-1}(1/3) < \theta < \sin^{-1}(1/2)$, only the second harmonic can radiate for this choice of θ, and the three values of the wall inclination $\alpha = 15°$, $35°$ and $65°$ in figure 8(*a–c*) correspond to the configurations shown in figure 4(*a–c*), respectively. Figure 8(*d*), on the other hand, illustrates a case when the angle of incidence ($\theta = 15°$) is in the range $\sin^{-1}(1/4) < \theta < \sin^{-1}(1/3)$ so both the second and third harmonics can radiate. To gain further quantitative insight, figure 9(*a–d*) shows cross-sections of the plots in figure 8(*a–d*) at a fixed distance from the wall.

The amplitudes of the various harmonics in expansion (3.7) were calculated from (3.9*a*), (3.14), (3.15), (3.23) and (3.24), using the fast Fourier transform to compute Fourier transforms and the trapezoidal rule for evaluating integrals. To ensure no reflection from the boundaries, a sufficiently large domain in the x-direction along the slope was employed. In validating the numerical procedure, the energy-balance

https://doi.org/10.1017/S0022112004002769 Published online by Cambridge University Press

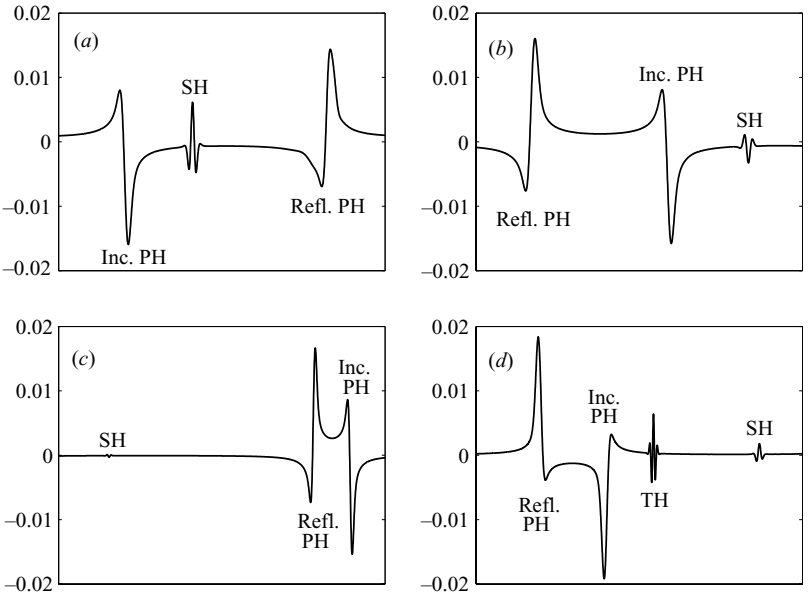

FIGURE 9. Streamfunction ψ at $t = 10$ along the cross-sections indicated by dashed lines in figure 8(*a–d*). PH, SH and TH stand for the primary, second and third harmonic, respectively.

equation (4.5) was used as a check. Moreover, doubling the spatial resolution had no appreciable effect on the results.

In the steady-state response discussed in § 3, the direction of each of the reflected beams relative to the incident beam was determined by invoking the radiation condition, ensuring that the reflected energy propagates outwards from the slope. As a result, under certain flow conditions, some of the reflected beams can be found on the opposite side of the vertical from the rest of their counterparts; for example, the reflected second-harmonic beam in figure 8(*b*) and the reflected second- and third-harmonic beams in figure 8(*d*) propagate upslope, while the primary-harmonic beam is reflected downslope in both these instances.

As an independent check of this interesting application of the radiation condition, adapting the numerical code used in Lamb (1994), we ran an unsteady simulation mimicking the steady-state response shown in figure 8(*b*) for a beam propagating at $\theta = 25^\circ$ to the horizontal and reflecting from a slope of inclination $\alpha = 35^\circ$. The numerical model solves the two-dimensional inviscid nonlinear equations of motion under the Boussinesq approximation. The incident wave beam was generated via a localized (in the form of a Gaussian) oscillatory forcing in the vertical direction that was turned on impulsively. A snapshot from this simulation after 20 oscillation periods of the forcing is shown in figure 10. While no quantitative comparison against the steady-state theory will be attempted here, a reflected second-harmonic beam propagating upslope is clearly seen in figure 10, and the reflected primary-harmonic beam is found on the downslope side of the incident beam, in accordance with the steady-state theory. There is also evidence from recent laboratory experiments, conducted by the first author (A.T.) and T. Peacock at MIT, that the second-harmonic beam propagates upslope in this flow geometry. These results will be reported elsewhere.

https://doi.org/10.1017/S0022112004002769 Published online by Cambridge University Press

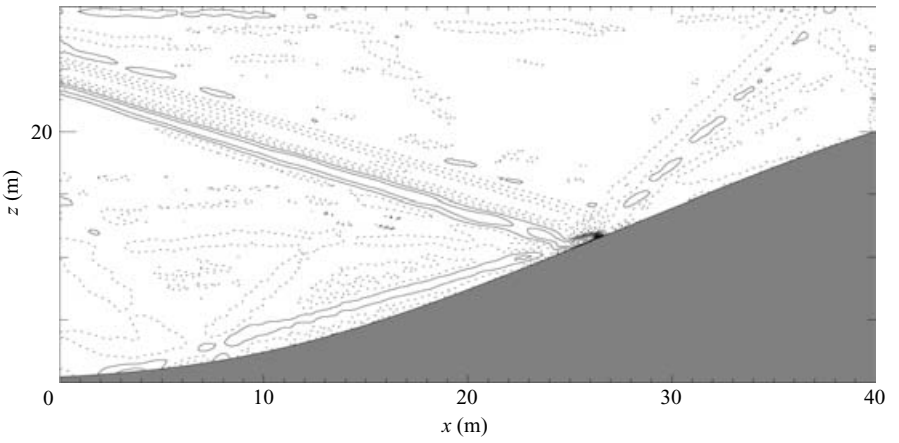

FIGURE 10. A snapshot of the horizontal velocity field from an unsteady simulation mimicking the steady-state response shown in figure 8(*b*) for a beam propagating at $\theta = 25^\circ$ to the horizontal and reflecting from a slope of inclination $\alpha = 35^\circ$.

Returning to figure 9(*a–c*), we remark that the reflected second-harmonic beam in 9(*c*), where the wall is closer to the vertical, is quite weak. To gain a more systematic understanding of the dependence of the reflected second-harmonic beam on the flow geometry, we investigated the behaviour of $\mathscr{F}_2^{\mathrm{refl}}/\mathscr{F}^{\mathrm{inc}}$, the ratio of the energy flow rate in the second-harmonic beam to the energy flow rate in the incident beam, when the angle of incidence θ and the wall inclination α are varied. According to (4.1) and (4.3), this ratio can be expressed as

$$\frac{|\mathscr{F}_2^{\mathrm{refl}}|}{|\mathscr{F}^{\mathrm{inc}}|} = \epsilon^2 \mathscr{F}_{21}, \tag{6.2a}$$

where

$$\mathscr{F}_{21} = \frac{\cos\gamma_2 \displaystyle\int_{-\infty}^{\infty} Q_2^{\mathrm{refl}^*} Q_{2x}^{\mathrm{refl}}\,\mathrm{d}x}{\cos\theta \displaystyle\int_{-\infty}^{\infty} Q^{\mathrm{inc}^*} Q_x^{\mathrm{inc}}\,\mathrm{d}x}, \tag{6.2b}$$

being independent of ϵ, controls the dependence on the flow geometry.

Figure 11(*a*) shows plots of $\mathscr{F}_{21}$ as a function of the wall inclination α for certain values of the angle of incidence θ, and figure 11(*b*) shows how $\mathscr{F}_{21}$ varies as a function of θ for fixed values of α. For a fixed value of θ, it is clear from figure 11(*a*) that the reflected second harmonic is relatively strong as long as α does not exceed significantly the critical angle ($\alpha = \theta$); as expected, $\mathscr{F}_{21}$ is singular when $\alpha = \theta$ but, quite remarkably, drops off rapidly as α is increased past this critical value. This explains the fact that the reflected second harmonic in figure 9(*c*) is so weak, given that $\theta = 25^\circ$ and $\alpha = 65^\circ$ in this case. On the other hand, as θ is varied for fixed α, $\mathscr{F}_{21}$ features an infinite peak at $\theta = \alpha$ only if $\alpha < \sin^{-1}(1/2)$, and, as shown in figure 11(*b*), the reflected second harmonic is most appreciable when θ is close to this peak. The maximum value of θ for which the second harmonic can radiate is $\sin^{-1}(1/2) = 30^\circ$.

6.2. *Colliding wave beams*

Following the same procedure as in § 6.1, here we compute steady-state wave patterns of colliding wave beams on the basis of expansion (5.1), correct to $O(\epsilon^3)$, for two

https://doi.org/10.1017/S0022112004002769 Published online by Cambridge University Press

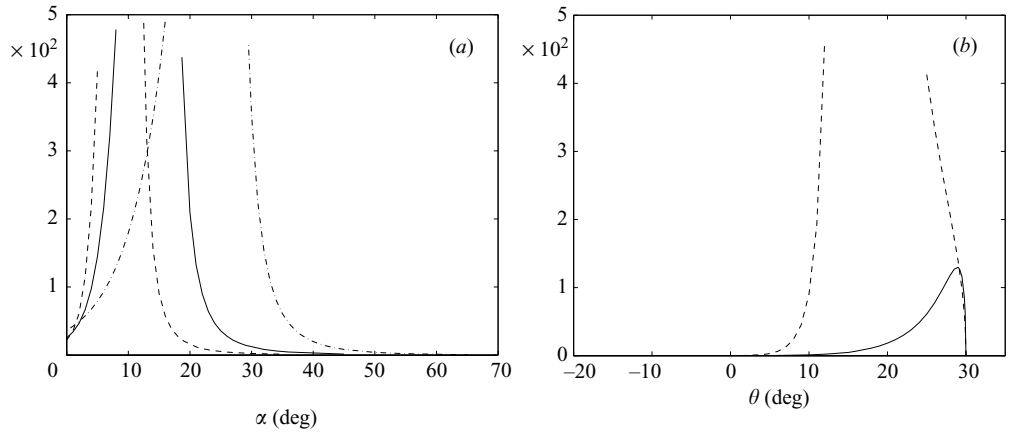

FIGURE 11. Plots of $\mathscr{F}_{21}$, where $\epsilon^2\mathscr{F}_{21}$ is the ratio of the energy flow rate in the second-harmonic beam to the energy flow rate in the incident beam: (*a*) wall inclination α varies for three fixed values of angle of incidence θ; $\theta = 10^\circ$ (– –), $\theta = 15^\circ$ (—), and $\theta = 25^\circ$ (–·–); (*b*) angle of incidence θ varies for fixed values of wall inclination $\alpha = 15^\circ$ (– –) and $\alpha = 35^\circ$ (—).

specific configurations: a beam propagating at $\theta = -25^\circ$ to the horizontal that collides obliquely with its second harmonic, a situation somewhat analogous to the collision highlighted in figure 1; and a more general collision involving a beam propagating at $\theta = -15^\circ$ and another propagating at $\phi = 40^\circ$ to the horizontal. Again, energy balance, correct to $O(\epsilon^4)$, within a large control volume enclosing the collision region has been used to verify the numerical results.

Figure 12 shows contour plots of the streamfunction ψ at $t = 10$, correct to $O(\epsilon^3)$, for these two collisions, and cross-sections of these plots along the dashed lines marked in figure 12 are illustrated in figure 13. In the first case, figure 12(*a*) shows an additional beam with frequency ω_θ emerging from the collision region along a different direction than those of the two colliding beams. This is reminiscent of the collision highlighted in figure 1, which involves beams with the background-flow frequency and its second harmonic, but the resemblance is merely qualitative given that the colliding beams in figure 1 have different profiles and quite lower frequencies than those in figure 12(*a*).

The effect of nonlinear interactions is much more dramatic in the collision shown in figure 12(*b*), where five additional beams are visible. It is worth noting that, for the relatively small value of amplitude parameter $\epsilon = 0.05$ used here, certain $O(\epsilon^3)$ beams are surprisingly strong while out of four $O(\epsilon^2)$ beams with frequency $\omega_\theta + \omega_\phi$ that can possibly be generated in this configuration according to figure 6(*e*), only one is strong enough to be visible in figure 12(*b*).

While no systematic study has been attempted here, the two examples of collisions in figure 12 suggest that the strength of the various nonlinear interactions, responsible for the generation of additional beams, depends in a serious way on the geometry and the particular profile of the colliding beams.

This work was supported by the Air Force Office of Scientific Research, Air Force Materials Command, USAF, under Grant F49620-01-1-001 and by the National Science Foundation Grants DMS-0072145 and DMS-0305940. KGL also wishes to acknowledge support from the Natural Sciences and Engineering Research Council of Canada.

https://doi.org/10.1017/S0022112004002769 Published online by Cambridge University Press

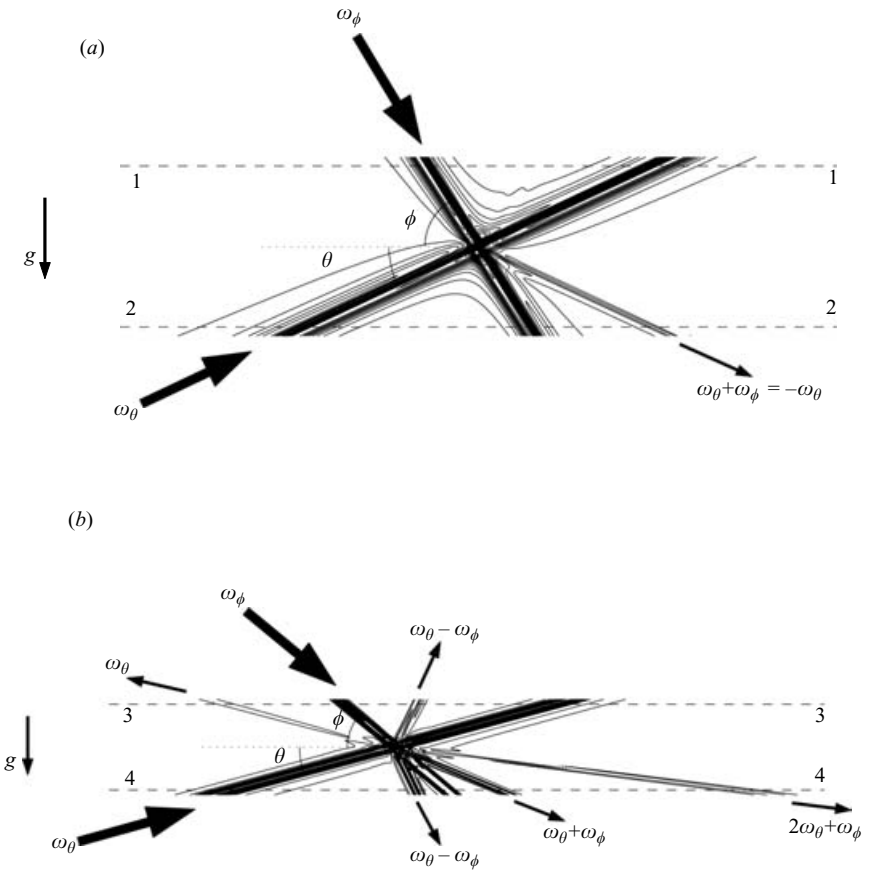

FIGURE 12. Contour plots of the streamfunction ψ at $t=10$ for two configurations of colliding wave beams: (*a*) $\theta=-25^\circ$ and $\phi=-\sin^{-1}(2\sin\theta)=57.7^\circ$; (*b*) $\theta=-15^\circ$ and $\phi=40^\circ$. Dashed lines (– –) indicate the cross-sections of these plots shown in figure 13.

Appendix A. Forcing terms of higher-order reflected disturbances

The explicit expressions for the forcing terms $f_n(x, y)$ $(n=1, 2, 3)$ in (3.10*a*) are

$$\begin{aligned} f_1(x, y) = {} & \cos\alpha\{J(R^*, Q_2)+J(R_2, Q^*)+J(R_0, Q)+J(R, Q_0)\}_x \\ & -\sin\alpha\{J(R^*, Q_2)+J(R_2, Q^*)+J(R_0, Q)+J(R, Q_0)\}_y \\ & -\mathrm{i}\sin\theta\{J(\nabla^2 Q^*, Q_2)+J(\nabla^2 Q_2, Q^*)+J(\nabla^2 Q_0, Q)+J(\nabla^2 Q, Q_0)\}, \end{aligned} \tag{A 1}$$

$$f_2(x, y) = -3\mathrm{i}\sin\theta\, J(\nabla^2 Q, Q), \tag{A 2}$$

$$\begin{aligned} f_3(x, y) = {} & \cos\alpha\{J(R, Q_2)+J(R_2, Q)\}_x - \sin\alpha\{J(R, Q_2)+J(R_2, Q)\}_y \\ & -3\mathrm{i}\sin\theta\{J(\nabla^2 Q, Q_2)+J(\nabla^2 Q_2, Q)\}. \end{aligned} \tag{A 3}$$

The forcing terms $h_n(x, y)$ $(n=1, 2, 3)$ in (3.11) are given by

$$h_1(x, y) = -\frac{\mathrm{i}}{\sin\theta}\{J(R^*, Q_2)+J(R_2, Q^*)+J(R_0, Q)+J(R, Q_0)\}, \tag{A 4}$$

$$h_2(x, y) = -\frac{1}{2\sin^2\theta}\{\cos\alpha\, J(Q_x, Q)-\sin\alpha\, J(Q_y, Q)\}, \tag{A 5}$$

$$h_3(x, y) = -\frac{\mathrm{i}}{3\sin\theta}\{J(R, Q_2)+J(R_2, Q)\}. \tag{A 6}$$

https://doi.org/10.1017/S0022112004002769 Published online by Cambridge University Press

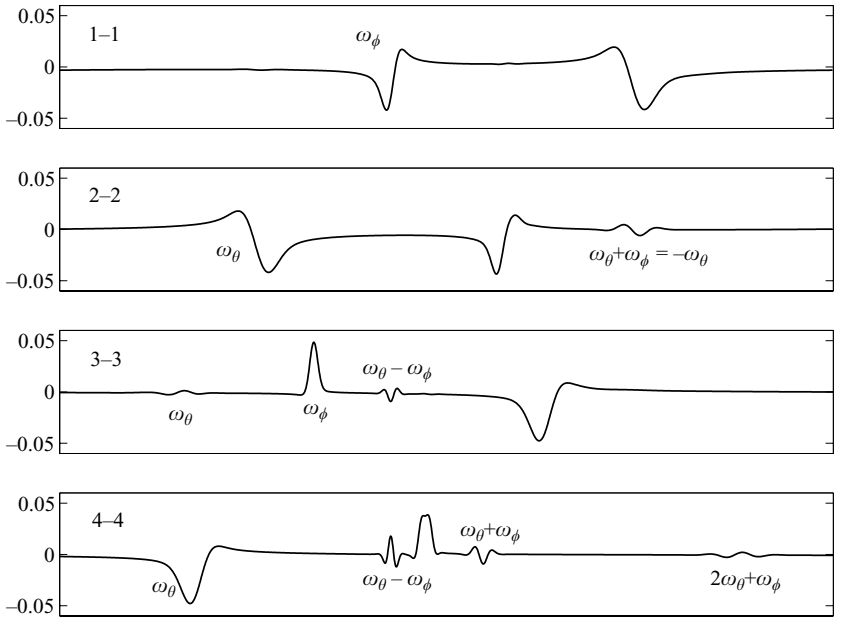

FIGURE 13. Streamfunction ψ at $t=10$ along the four cross-sections indicated by dashed lines in figure 12(a–b).

Appendix B. The $O(\epsilon^3)$ harmonics $2\omega_\theta \pm \omega_\phi$ and $\omega_\theta \pm 2\omega_\phi$ generated by nonlinear interactions of colliding wave beams

The harmonics $2\omega_\theta \pm \omega_\phi$ and $\omega_\theta \pm 2\omega_\phi$ satisfy the following forced problems

$$(2\omega_\theta \pm \omega_\phi)^2\, Q_{yy}^{2\theta\pm\phi} - \{1-(2\omega_\theta \pm \omega_\phi)^2\}\, Q_{xx}^{2\theta\pm\phi} = \Re^{2\theta\pm\phi}, \tag{B 1a}$$

$$(\omega_\theta \pm 2\omega_\phi)^2\, Q_{yy}^{\theta\pm2\phi} - \{1-(\omega_\theta \pm 2\omega_\phi)^2\}\, Q_{xx}^{\theta\pm2\phi} = \Re^{\theta\pm2\phi}, \tag{B 1b}$$

where

$$\begin{aligned}\Re^{2\theta\pm\phi} &= \{J(R^\theta, Q^\pm) + J(R^\pm, Q^\theta)\}_x \\ &\quad - \mathrm{i}(2\omega_\theta \pm \omega_\phi)\{J(\nabla^2 Q^\theta, Q^\pm) + J(\nabla^2 Q^\pm, Q^\theta)\},\end{aligned} \tag{B 2a}$$

$$\begin{aligned}\Re^{\theta+2\phi} &= \{J(R^\phi, Q^+) + J(R^+, Q^\phi)\}_x \\ &\quad - \mathrm{i}(\omega_\theta + 2\omega_\phi)\{J(\nabla^2 Q^\phi, Q^+) + J(\nabla^2 Q^+, Q^\phi)\},\end{aligned} \tag{B 2b}$$

and

$$\begin{aligned}\Re^{\theta-2\phi} &= \{J(R^{\phi^*}, Q^-) + J(R^-, Q^{\phi^*})\}_x \\ &\quad - \mathrm{i}(\omega_\theta - 2\omega_\phi)\{J(\nabla^2 Q^{\phi^*}, Q^-) + J(\nabla^2 Q^-, Q^{\phi^*})\}.\end{aligned} \tag{B 2c}$$

These problems may be solved following the same procedure as those in § 5.1 for $Q^\pm$.

REFERENCES

BELL, T. H. 1975 Lee waves in stratified flows with simple harmonic time dependence. *J. Fluid Mech.* **67**, 705–722.

CHASHECHKIN, Y. D. & NEKLYUDOV, V. I. 1990 Nonlinear interaction of bundles of short two-dimensional monochromatic internal waves in an exponentially stratified liquid. *Dokl. Earth Sci. Sect.* **311**, 235–238.

https://doi.org/10.1017/S0022112004002769 Published online by Cambridge University Press

Dauxois, T. & Young, W. R. 1999 Near-critical reflection of internal waves. *J. Fluid Mech.* **390**, 271–295.

Javam, A., Imberger, J. & Armfield, S. W. 1999 Numerical study of internal wave reflection from sloping boundaries. *J. Fluid Mech.* **396**, 183–201.

Javam, A., Imberger, J. & Armfield, S. W. 2000 Numerical study of internal wave–wave interactions in a stratified fluid. *J. Fluid Mech.* **415**, 65–87.

Kistovich, A. V. & Chashechkin, Y. D. 1991 Nonlinear interaction of two-dimensional packets of monochromatic internal waves. *Izv. Atmos. Ocean. Phys.* **27**, 946–951.

Lamb, K. G. 1994 Numerical experiments of internal wave generation by strong tidal flow across a finite amplitude bank edge. *J. Geophys. Res.* **99**, 843–864.

Lamb, K. G. 2004 Nonlinear interaction among internal wave beams generated by tidal flow over supercritical topography. *Geophys. Res. Lett.* **31**, DOI: 10.1029/2003GL019393.

Lighthill, M. J. 1978 *Waves in Fluids*. Cambridge University Press.

Phillips, O. M. 1966 *The Dynamics of the Upper Ocean*. Cambridge University Press.

Tabaei, A. & Akylas, T. R. 2003 Nonlinear internal gravity wave beams. *J. Fluid Mech.* **482**, 141–161.

Teoh, S. G., Ivey, G. N. & Imberger, J. 1997 Laboratory study of interaction between two internal wave rays. *J. Fluid Mech.* **336**, 91–122.

Thorpe, S. A. 1987 On the reflection of a train of finite amplitude internal waves from a uniform slope. *J. Fluid Mech.* **178**, 279–302.

https://doi.org/10.1017/S0022112004002769 Published online by Cambridge University Press